arXiv:1210.6756v1 [hep-ph] 25 Oct 2012

Top-seesaw assisted technicolor model and a $m = 126$ GeV scalar

Hidenori S. Fukano* and Kimmo Tuominen†
Department of Physics, University of Jyväskylä,
P.O.Box 35, FIN-40014 Jyväskylä, Finland
and Helsinki Institute of Physics, P.O.Box 64,
FIN-00014 University of Helsinki, Finland

We consider a model of strong dynamics able to account for the origin of the electroweak symmetry breaking and heavy quark masses. The model is based on a technicolor sector, augmented with topcolor and top-seesaw mechanism to assist in the generation of heavy quark masses. The low energy effective theory is a particular three Higgs doublet model. The additional feature is the possibility of the existence of composite higher spin states beyond the scalars, which are shown to be essential in this model to provide extra contributions in the higgs decays into two photons. We provide a detailed strategy and analysis how this type of models are to be constrained with the present data.

I. INTRODUCTION

The ATLAS [1] and CMS [2] experiments at LHC have announced a discovery of a new boson with mass $M_h \simeq 126$ GeV. The decay and production rates of this new particle appear to be consistent with the prediction of the Standard Model (SM) of elementary particle interactions, and therefore the next logical step is to try to uncover its properties more precisely and to see how well it fits in with various extensions of the Standard Model. For examples, see e.g. [3–12].

Strong dynamics remains as a viable alternative, although the discovery of a light scalar particle is a severe obstruction for traditional Technicolor models [13, 14]. Moreover, technicolor alone does not provide a mechanism to generate masses for the elementary matter fermions, and one must invoke more complex dynamical mechanisms.

How does a light scalar emerge from strongly coupled dynamics ? There are generally at least two different alternatives. First possibility arises, if the theory underlying the dynamical electroweak symmetry breaking is quasiconformal [15–18]. This means that under the renormalization group evolution the theory approaches an infrared fixed point which, however, is supercritical with respect to chiral symmetry breaking; formation of fermion-antifermion condensate triggers electroweak symmetry breaking and the theory flows into QCD like vacuum in the deep infrared. However, due to the presence of a quasi stable infrared fixed point the coupling constant evolves very slowly, i.e. walks, over a large hierarchy of scales and this quasiconformal behavior is directly reflected on the properties of the spectrum [19, 20]. The second alternative is that the contributions to the electroweak sector are shared beteween different sectors, i.e. there exists different scales, say v_1 and v_2 which together give $v_{\rm weak}^2 = v_1^2 + v_2$, but both v_1 and v_2 can be less than $v_{\rm weak}$. The masses of the excitations in different sectors are dictated by the scales v_1 and v_2, and hence these mass scales can also be smaller than $v_{\rm weak}$. This latter possibility will be considered in this paper.

Models of this type are motivated by the need to explain both the generation of the masses of the electroweak gauge bosons as well as the masses of the elementary fermion fields of the SM. We assume that the light fermion masses are explained by some Extended Technicolor (ETC) scenario [21], while the masses of the third generation quarks arise dominantly from additional strong dynamics, which we assume to be of top-seesaw type [22–24] in [25, 26].

The top-seesaw sector in this model is based on [24]. The basic idea of this model building is to introduce new vectorlike quarks not charged under the weak interaction, but which generate a nontrivial vacuum condensate via new strong dynamics shared between the third and fourth generation quarks. Concretely, under SU(3)$_1$×SU(3)$_2$× SU$_L$×U(1)$_1$×U(1)$_2$, these fields transform as

$$\begin{aligned} Q_L^{(3)} &\sim (3,1,2,1/6,0), \quad U_R^{(3)} \sim (1,1,3,1,0,2/3), \quad U_R^{(3)} \sim (1,1,3,1,0,-1/3) \\ U_L^{(4)} &\sim (1,1,3,1,0,2/3), \quad U_R^{(4)} \sim (1,3,1,1,2/3,0), \quad D_L^{(4)} \sim (1,1,3,1,0,-1/3), \quad D_R^{(4)} \sim (1,3,1,1,-1/3,0). \end{aligned} \quad (1)$$

---

*Electronic address: hidenori.f.sakuma@jyu.fi
†Electronic address: kimmo.i.tuominen@jyu.fi

The full underlying gauge symmetry is assumed to reduce to $\mathrm{SU}(3)_{\mathrm{QCD}}\times\mathrm{SU}(2)_L\times\mathrm{U}(1)_Y$ via symmetry breaking at scale $\Lambda \gg v_{\mathrm{weak}}$, generating effective four fermion interactions

$$\mathcal{L}^{4f} = G_b\left(\bar{D}_R^{(4)}Q_L^{(3)}\right)^2 + G_t\left(\bar{U}_R^{(4)}Q_L^{(3)}\right)^2 + G_{tb}\left(\bar{Q}_L^{(3)}U_R^{(4)}\right)\left(\bar{D}_R^{(4)c}i\tau_2 Q_L^{(3)c}\right) , \tag{2}$$

where the superscript ^{c} implies charge conjugation. The diagonal terms, G_b and G_t arise from the exchange of eight colored gauge bosons with mass $\sim \Lambda$. The off diagonal term G_{tb} may arise either from FCNC interactions of the topcolor [27] sector or via the topcolor instantons [24].

The above four-fermion interactions, when strong, lead to vacuum condensates of the form $\bar{D}_R^{(4)}Q_L^{(3)}$ and $\bar{U}_R^{(4)}Q_L^{(3)}$, and these contribute to electroweak symmetry breaking and to the masses of heavy quarks. The quark mass spectrum is fully specified by noting that in addition to the dynamically generated quark masses Σ_U and Σ_D, the low energy gauge invariance also allows for the mass terms $M_U^{(43)}\bar{U}_L^{(4)}U_R^{(3)}$ and $M_U^{(44)}\bar{U}_L^{(4)}U_R^{(4)}$ and similarly with the replacement $U \to D$. The quark mass spectrum is then determined from

$$\mathcal{L}_M = -(\bar{U}_L^{(3)}, \bar{U}_L^{(4)})\begin{pmatrix} 0 & \Sigma_U \\ M_U^{(43)} & M_U^{(44)} \end{pmatrix}\begin{pmatrix} U_R^{(3)} \\ U_R^{(4)} \end{pmatrix} - (\bar{D}_L^{(3)}, \bar{D}_L^{(4)})\begin{pmatrix} 0 & \Sigma_D \\ M_D^{(43)} & M_D^{(44)} \end{pmatrix}\begin{pmatrix} D_R^{(3)} \\ D_R^{(4)} \end{pmatrix} + \text{h.c.}. \tag{3}$$

From the structure of the condensates, it follows that the top-seesaw sector is, at low energies, described by an effective two-higgs doublet model. As in [26], we consider also an underlying (extended) technicolor sector responsible for the electroweak symmetry breaking, but contributing only in subleading order to the heavy quark masses. The light fermion masses are expected to be generated by the extended technicolor interactions. Considering technicolor and top-seesaw dynamics together then leads to a three-doublet model as an effective low energy description of the strong dynamics.

In [26] we considered a concrete model built upon the minimal walking technicolor [19, 20] model. Here, we keep the technicolor sector generic, with the chiral symmetry $\mathrm{SU}(2)_L\times$ $\mathrm{SU}(2)_R$ chiral symmetry whose spontaneous breaking contributes to electroweak symmetry breaking. When comparing with precision data, we also outline how different technicolor models, like the minimal walking technicolor, affect the results.

The paper is organized as follows: First we introduce the low energy Lagrangian in section II . Then, in section III we compute the spectrum of fermions and composite particles. The constraints from electroweak precision observables are considered in section IV, and finally in section V we consider the model in light of the recent LHC data.

II. LOW ENERGY EFFECTIVE LAGRANGIAN

In this section, we consider the low energy effective theory for the top-seesaw assisted TC model. To describe the Nambu-Goldstone bosons (NGBs) of the TC sector, we use the most minimal electroweak chiral Lagrangian (EWCL) [28–30] based on the $G/H = [SU(2)_L \times SU(2)_R]/SU(2)_V$, which is the most minimal structure. In other words, the leading order chiral Lagrangian is

$$\mathcal{L}^{(2)}_{\mathrm{EWCL}} = |D_\mu\Phi_{\mathrm{TC}}|^2 , \tag{4}$$

where Φ_{TC} is given by

$$\Phi_{\mathrm{TC}} = \begin{pmatrix} \pi^+_{\mathrm{TC}} \\ \frac{1}{\sqrt{2}}\left[v_{\mathrm{TC}} - i\pi^0_{\mathrm{TC}}\right] \end{pmatrix} , \tag{5}$$

and $\tilde{\Phi}_{\mathrm{TC}} \equiv i\tau^2\Phi^*_{\mathrm{TC}}$, where τ^2 is the second Pauli matrix. The covariant derivative $D_\mu\Phi_{\mathrm{TC}}$ is given by

$$D_\mu\Phi_{\mathrm{TC}} = \partial_\mu\Phi_{\mathrm{TC}} - igW^a_\mu T^a\Phi_{\mathrm{TC}} - \frac{1}{2}g'B_\mu\Phi_{\mathrm{TC}} , \tag{6}$$

where $T^a = (1/2)\tau^a$ and W_μ, B_μ are the SM $SU(2)_L, U(1)_Y$ gauge boson fields and g, g' are their gauge couplings. On the other hand, the top-seesaw sector is described by the two higgs doublet model (2HDM) [24], i.e. by doublets $\Phi_i\,(i = 1, 2)$

$$\Phi_i = \begin{pmatrix} \pi^+_i \\ \frac{1}{\sqrt{2}}\left[v_i + h^0_i - i\pi^0_i\right] \end{pmatrix} , \tag{7}$$

and the covariant derivatives for Φ_i under the electroweak gauge symmetry are as in Eq.(6). Thus the low energy effective Lagrangian of the top-seesaw assisted TC model is given by

$$\mathcal{L}_{\rm higgs}(\Phi_1,\Phi_2,\Phi_{\rm TC}) = \sum_{i=1,2,{\rm TC}} |D_\mu \Phi_i|^2 + \mathcal{L}_{\rm yukawa} - V(\Phi_1,\Phi_2,\Phi_{\rm TC})\,. \tag{8}$$

Here, $\mathcal{L}_{\rm yukawa}$ consists of the Yukawa interaction terms and is given explicitly by

$$\begin{aligned}\mathcal{L}_{\rm yukawa} = &-\sum_{i,j=1,2,3}^{\rm quarks} y^{(d)}_{ij}\bar{Q}^{(i)}_L \Phi_{\rm TC} D^{(j)}_R - \sum_{i,j=1,2,3}^{\rm quarks} y^{(u)}_{ij}\bar{Q}^{(i)}_L \tilde{\Phi}_{\rm TC} U^{(j)}_R \\ &-y_1 \bar{Q}^{(3)}_L \Phi_1 D^{(4)}_R - y_2 \bar{Q}^{(3)}_L \tilde{\Phi}_2 U^{(4)}_R \\ &+{\rm h.c.}\,. \end{aligned}\tag{9}$$

Note here that the implications from the Yukawa term in Eq.(9) are very different from the usual 2HDM [31]. This is so since the neutral higgs boson h^0 arises only from the doublets $\Phi_{1,2}$ of Eqs.(5) and (7), does not couple to any leptons or any light quarks at tree level. Therefore, for the phenomenological purposes we will concentrate only on the quark sector and we will omit the light generations in what follows. Also note that due to this underlying structure, the FCNC problem of the generic 2HDM is completely avoided in our model.

The potential $V(\Phi_1,\Phi_2,\Phi_{\rm TC})$ in Eq.(8) arising from the top-seesaw sector can be decomposed as

$$V(\Phi_1,\Phi_2,\Phi_{\rm TC}) = V_{\rm TSS}(\Phi_1,\Phi_2) + V_M(\Phi_1,\Phi_2,\Phi_{\rm TC})\,. \tag{10}$$

We take $V_{\rm TSS}(\Phi_1,\Phi_2)$ to be of the form

$$\begin{aligned}V_{\rm TSS}(\Phi_1,\Phi_2) \;=\; & M^2_{11}|\Phi_1|^2 + M^2_{22}|\Phi_2|^2 - M^2_{12}\left[\Phi_1^\dagger\Phi_2 + {\rm h.c.}\right] \\ &+\frac{1}{2}\lambda_1(\Phi_1^\dagger\Phi_1)^2 + \frac{1}{2}\lambda_2(\Phi_2^\dagger\Phi_2)^2 + \lambda_3(\Phi_1^\dagger\Phi_1)(\Phi_2^\dagger\Phi_2) + \lambda_4(\Phi_1^\dagger\Phi_2)(\Phi_2^\dagger\Phi_1)\,.\end{aligned}\tag{11}$$

All these terms are generated by the underlying theory via the four fermion interactions (2).

Note that this scalar potential for top-seesaw sector in Eq.(11) is different from the scalar potential given in [24, 26]. In [24, 26], there are $[\lambda_6(\Phi_1^\dagger\Phi_1) + \lambda_7(\Phi_2^\dagger\Phi_2)](\Phi_1^\dagger\Phi_2) + {\rm h.c.}]$-terms, which arise from the Peccei-Quinn (PQ) $U(1)_A$ symmetry is breaking topcolor instanton induced four fermion interaction. Here, on the other hand, we do not specify the PQ-symmetry breaking mechanism, but assume instead that PQ- symmetry breaks by M^2_{12}-term derived from the last term in Eq.(2) [32–34]. In comparison to generic two-doublet models we remark, that the potential Eq.(11) is derived by the bubble-sum approximation [35] from the microscopic Lagrangian (2), and hence does not include $\lambda_5[(\Phi_1^\dagger\Phi_2)^2 + {\rm h.c.}]$ term [26, 34].

To account for the mixing between the TC sector and the top-seesaw sector, we have added $V_M(\Phi_1,\Phi_2,\Phi_{\rm TC})$ to the 2HDM potential Eq.(11) in Eq.(10). This contribution is given by [36]

$$V_M(\Phi_1,\Phi_2,\Phi_{\rm TC}) = c_1 v_1^2\left|\Phi_1 - \frac{v_1}{v_{\rm TC}}\Phi_{\rm TC}\right|^2 + c_2 v_2^2\left|\Phi_2 - \frac{v_2}{v_{\rm TC}}\Phi_{\rm TC}\right|^2\,, \tag{12}$$

where $c_{1,2}$ are dimensionless parameters. This additional potential, Eq.(12), does not contribute to the stationarity conditions, determined by the potential Eq.(11). The vacuum structure of this model is determined by three vacuum expectation values (vevs), $v_{{\rm TC},1,2}$, all contributing to the electroweak symmetry breaking, and satisfying the constraint $v_1^2 + v_2^2 + v_{\rm TC}^2 = v_{\rm EW}^2$, where $v_{\rm EW} = 246\,({\rm GeV})$. We define $\tan\beta$ and $\tan\phi$ as

$$\tan\beta \equiv \frac{v_2}{v_1} \quad , \quad \tan^2\phi \equiv \frac{v_{\rm TC}^2}{v_1^2 + v_2^2}\,, \tag{13}$$

or in other words,

$$\begin{aligned} v_{\rm TC} &= v_{\rm EW}\sin\phi, \\ v_1 &= v_{\rm EW}\cos\phi\cos\beta, \\ v_2 &= v_{\rm EW}\cos\phi\sin\beta. \end{aligned}\tag{14}$$

Next, we discuss the higgs boson mass spectrum in the present model. The quadratic terms of the NGB fields arising from the both sectors,$V(\Phi_1,\Phi_2)+V_M(\Phi_1,\Phi_2,\Phi_{\rm TC})$, are given by

$$\mathcal{L}^{\rm higgs} = -\frac{1}{2}(\pi_1^0\ \ \pi_2^0\ \ \pi_{\rm TC}^0)\mathcal{M}_\pi^2\begin{pmatrix}\pi_1^0\\ \pi_2^0\\ \pi_{\rm TC}^0\end{pmatrix} - (\pi_1^+\ \ \pi_2^+\ \ \pi_{\rm TC}^+)\mathcal{M}_{\pi\pm}^2\begin{pmatrix}\pi_1^-\\ \pi_2^-\\ \pi_{\rm TC}^-\end{pmatrix} - \frac{1}{2}(h_1^0\ \ h_2^0)\mathcal{M}_h^2\begin{pmatrix}h_1^0\\ h_2^0\end{pmatrix}. \tag{15}$$

Let us first concentrate for the top-seesaw sector only. Then the CP-odd higgs and charged higgs mass matrices are given by [37]

$$\mathcal{M}_\pi^2|_{\rm TC=0} = M_{12}^2\begin{pmatrix}\tan\beta & -1\\ -1 & \tan\beta\end{pmatrix} \tag{16}$$

for the CP-odd higgs sector, and

$$\mathcal{M}_{\pi\pm}^2|_{\rm TC=0} = \left[M_{12}^2 - \frac{1}{2}\lambda_4 v_{\rm EW}^2\cos^2\phi\sin\beta\cos\beta\right]\begin{pmatrix}\tan\beta & -1\\ -1 & \tan\beta\end{pmatrix} \tag{17}$$

for the charged higgs sector. It will be convenient to define $M^2_{\rm TSS,0,\pm}$ as

$$M^2_{\rm TSS,0} = \frac{M_{12}^2}{\cos\beta\sin\beta} \quad , \quad M^2_{\rm TSS,\pm} = M^2_{\rm TSS,0} - \frac{1}{2}\lambda_4 v_{\rm EW}^2\cos^2\phi\,, \tag{18}$$

which are eigenvalues of Eqs.(16) and (17). In our study we will treat $M_{\rm TSS,0}$ as a free parameter. The CP-even higgs boson mass matrices are given by

$$\mathcal{M}_h^2 = M^2_{\rm TSS,0}\begin{pmatrix}\sin^2\beta & -\sin\beta\cos\beta\\ -\sin\beta\cos\beta & \cos^2\beta\end{pmatrix} + v_{\rm EW}^2\cos^2\phi\begin{pmatrix}2\lambda_1\cos^2\beta & (\lambda_3+\lambda_4)\sin\beta\cos\beta\\ (\lambda_3+\lambda_4)\sin\beta\cos\beta & 2\lambda_2\sin^2\beta\end{pmatrix}. \tag{19}$$

The CP-even higgs boson (h^0, H^0) masses, $m_h < m_H$, are eigenvalues of Eq. (19). They are determined solely by the top-seesaw sector, since the TC sector is described by a "higgsless" doublet. The mixing angle in the CP-even higgs boson sector is defined as

$$\tan(2\alpha) = \frac{2[\mathcal{M}_h^2]_{12}}{[\mathcal{M}_h^2]_{11}-[\mathcal{M}_h^2]_{22}}\,, \quad \text{with } -\frac{\pi}{2}\le\alpha\le 0\,, \tag{20}$$

and the two CP-even higgs boson mass eigenstates are given by

$$\begin{pmatrix}H^0\\ h^0\end{pmatrix} = \begin{pmatrix}\cos\alpha & \sin\alpha\\ -\sin\alpha & \cos\alpha\end{pmatrix}\begin{pmatrix}h_1^0\\ h_2^0\end{pmatrix}, \tag{21}$$

which is the same as in the usual 2HDM. However, we should note the meaning of α in the present model. From Eqs. (9) and (21), we deduce that the two CP-even higgs bosons couple to fermions as

$$[H^0\bar{D}_L^{(3)}D_R^{(4)}\,,\,h^0\bar{U}_L^{(3)}U_R^{(4)}]\text{-couplings}\propto(\cos\alpha)\quad,\quad[h^0\bar{D}_L^{(3)}D_R^{(4)}\,,\,H^0\bar{U}_L^{(3)}U_R^{(4)}]\text{-couplings}\propto(\sin\alpha)\,. \tag{22}$$

Generally the coupling between the composite higgs and its constituent fermions is strong. Therefore, looking at the above couplings, we find that if $|\tan\alpha| < 1$, the composite higgs h^0 is dominantly a fluctuation of the condensate of up-type quarks. Similarly, if $\tan\alpha| > 1$, h^0 consists dominantly of a fluctuation around the condensate of down-type quarks. Consequently, we can estimate constituent fermion species of the light CP-even higgs boson via the value of $\cos\alpha$.

Then, taking into account the mixing between the top-seesaw sector and TC sector, the mass matrix of the neutral CP-odd higgs boson fields, $\pi_i^0, (i=1,2,{\rm TC})$, including the neutral top-pion of the top-seesaw sector and techni-pion of TC sector, is

$$\mathcal{M}_\pi^2 = \left(\begin{array}{cc|c} \multicolumn{2}{c|}{\multirow{2}{*}{$\mathcal{M}_\pi^2|_{\rm TC=0}$}} & 0\\ & & 0\\ \hline 0 & 0 & 0\end{array}\right) + \begin{pmatrix}c_1v_1^2 & 0 & -M_1^2\\ 0 & c_2v_2^2 & -M_2^2\\ -M_1^2 & -M_2^2 & M_1^2\cos\beta\cot\phi + M_2^2\sin\beta\cot\phi\end{pmatrix}. \tag{23}$$

Similarly, the mass matrix of charged higgs boson field, $\pi_i^\pm$, which includes the charged top-pion and charged technipion, is

$$\mathcal{M}^2_{\pi^\pm} = \left(\begin{array}{cc|c} \multicolumn{2}{c|}{\mathcal{M}^2_{\pi^\pm}\big|_{\rm TC=0}} & \begin{matrix} 0 \\ 0 \end{matrix} \\ \hline 0 & 0 & 0 \end{array}\right) + \begin{pmatrix} c_1 v_1^2 & 0 & -M_1^2 \\ 0 & c_2 v_2^2 & -M_2^2 \\ -M_1^2 & -M_2^2 & M_1^2\cos\beta\cot\phi + M_2^2\sin\beta\cot\phi \end{pmatrix} . \tag{24}$$

In the above equations, we have defined the mixing mass term between top-seesaw sector and TC sector in $V_M(\Phi_1, \Phi_2, \Phi_{\rm TC})$ as

$$M_1^2 = c_1 v_1^2 \frac{v_1}{v_{\rm TC}} \quad , \quad M_2^2 = c_2 v_2^2 \frac{v_2}{v_{\rm TC}} . \tag{25}$$

The CP-odd and charged higgs bosons are represented in terms of the mass basis as

$$\begin{pmatrix} G^0 \\ A_2^0 \\ A_1^0 \end{pmatrix} = O_0^T \begin{pmatrix} \pi_1^0 \\ \pi_2^0 \\ \pi_{\rm TC}^0 \end{pmatrix} \quad , \quad \begin{pmatrix} G^\pm \\ H_2^\pm \\ H_1^\pm \end{pmatrix} = \mathcal{O}_\pm^T \begin{pmatrix} \pi_1^\pm \\ \pi_2^\pm \\ \pi_{\rm TC}^\pm \end{pmatrix} , \tag{26}$$

where the orthogonal matrix O_p ($p = 0, \pm$) is given as [34]

$$O_p = \begin{pmatrix} \cos\phi\cos\beta & -\sin\beta\cos\zeta_p + \sin\phi\cos\beta\sin\zeta_p & -\sin\beta\sin\zeta_p - \sin\phi\cos\beta\cos\zeta_p \\ \cos\phi\sin\beta & \cos\beta\cos\zeta_p + \sin\phi\sin\beta\sin\zeta_p & \cos\beta\sin\zeta_p - \sin\phi\sin\beta\cos\zeta_p \\ \sin\phi & -\cos\phi\sin\zeta_p & \cos\phi\cos\zeta_p \end{pmatrix} . \tag{27}$$

The states $G^{0,\pm}$ become the longitudinal components of the weak gauge bosons and the corresponding mass eigenvalues are $M^2_{G^{0,\pm}} = 0$. The non-zero eigenvalues are given as

$$\begin{aligned} 2\hat{M}^2_{S_2} &= M^2_{{\rm TSS},p} + \frac{(\sin^2\phi + \cos^2\beta\cos^2\phi)M_1^2}{\cos\beta\cos\phi\sin\phi} + \frac{(\sin^2\phi + \sin^2\beta\cos^2\phi)M_2^2}{\sin\beta\cos\phi\sin\phi} \\ &\quad - \left[\begin{array}{l} \dfrac{4}{\cos^2\phi}\left(M_1^2\sin\beta - M_2^2\cos\beta\right)^2 \\ + \left\{ M^2_{{\rm TSS},p} + \dfrac{(\sin^2\beta\sin^2\phi - \cos^2\beta)M_1^2}{\cos\beta\cos\phi\sin\phi} + \dfrac{(\cos^2\beta\sin^2\phi - \sin^2\beta)M_2^2}{\sin\beta\cos\phi\sin\phi} \right\}^2 \end{array} \right]^{1/2} , \end{aligned} \tag{28}$$

$$\begin{aligned} 2\hat{M}^2_{S_1} &= M^2_{{\rm TSS},p} + \frac{(\sin^2\phi + \cos^2\beta\cos^2\phi)M_1^2}{\cos\beta\cos\phi\sin\phi} + \frac{(\sin^2\phi + \sin^2\beta\cos^2\phi)M_2^2}{\sin\beta\cos\phi\sin\phi} \\ &\quad + \left[\begin{array}{l} \dfrac{4}{\cos^2\phi}\left(M_1^2\sin\beta - M_2^2\cos\beta\right)^2 \\ + \left\{ M^2_{{\rm TSS},p} + \dfrac{(\sin^2\beta\sin^2\phi - \cos^2\beta)M_1^2}{\cos\beta\cos\phi\sin\phi} + \dfrac{(\cos^2\beta\sin^2\phi - \sin^2\beta)M_2^2}{\sin\beta\cos\phi\sin\phi} \right\}^2 \end{array} \right]^{1/2} , \end{aligned} \tag{29}$$

where $S = A^0, H^\pm$ and $p = 0, \pm$, respectively. The mixing angle $\tan\zeta_p$ is defined as

$$\tan\zeta_p = \frac{\hat{M}^2_{S_2}\cos\phi\sin\phi - \left(M_1^2\cos\beta + M_2^2\sin\beta\right)}{\sin\phi\,(M_1^2\sin\beta - M_2^2\cos\beta)} . \tag{30}$$

To obtain more insight into this spectrum, we briefly consider the case with $c_1 = c_2 = 0$. This basically corresponds to the case studied in [26]. In this case, $\begin{pmatrix} G & S_2 & S_1 \end{pmatrix}^T$ becomes

$$\begin{pmatrix} G \\ S_2 \\ S_1 \end{pmatrix} = \begin{pmatrix} \cos\phi\cos\beta & \cos\phi\sin\beta & \sin\phi \\ \sin\phi\cos\beta & \sin\phi\sin\beta & -\cos\phi \\ -\sin\beta & \cos\beta & 0 \end{pmatrix} \begin{pmatrix} \pi_1 \\ \pi_2 \\ \pi_{\rm TC} \end{pmatrix} . \tag{31}$$

From Eqs.(28), (29) and (31) with $c_1 = c_2 = 0$ one can easily see that S_1, not S_2, corresponds to the CP-odd higgs bosons in the 2HDM with $M_S^2 = M_{\rm TSS,p}^2$. On the other hand the S_2 becomes massless. To resolve this, we note that TC sector contributes to $\pi_{\rm TC}$ through ETC interactions. Hence, on the effective theory level, we should add a mass term for $\pi_{\rm TC}$,

$$\mathcal{L}_{\rm ETC}^{\rm mass} = -m_{\rm ETC}^2 \left[\frac{1}{2}\pi_{\rm TC}^0\pi_{\rm TC}^0 + \pi_{\rm TC}^+\pi_{\rm TC}^-\right] , \tag{32}$$

with the value of $m_{\rm ETC}^2$ larger than the difference of the mass eigenvalues give by Eqs. (28) and (29). This will give a large contribution to mass of S_2 but a negligible contribution to mass of S_1. In other words, we arrange the spectrum so that mass squared of the state S_1 is given by Eq. (29), while the mass squared of S_2 is given by the sum of Eq. (28) and $m_{\rm ETC}^2$. The Goldstone boson G which is absorbed by the electroweak gauge boson of course remains massless. Evidently, we do not know $m_{\rm ETC}$ quantitatively unless we consider a concrete ETC model. In this paper we will set $m_{\rm ETC} = \Lambda_{\rm TC} = 4\pi v_{\rm TC}$ corresponding to the cutoff scale for the non-linear sigma model which we use to describe the TC sector.

III. RENORMALIZATION GROUP EQUATIONS AND THE COMPOSITENESS CONDITIONS

In the previous paper [26], we analyzed the dynamics by using the gap equations. In order to carry out more precise analysis in this paper, we study the model using the renormalization group equations (RGEs) together with compositness conditions [35]. We ignore the RGEs of SM electroweak interaction since their contributions are negligible at the relevant energy scales, and consider only the RGEs for QCD gauge coupling, Yukawa couplings and the higgs quartic couplings. The RGE for $SU(3)_c$ gauge coupling is given by

$$(16\pi^2)\mu\frac{dg_3}{d\mu} = -\left[11 - \frac{4}{3}N_g\right] g_3^3 , \tag{33}$$

with the initial condition $\alpha_{\rm QCD}(M_Z^2) \equiv g_3^2(M_Z^2)/(4\pi^2) = 0.1184$. Here N_g is number of fermion generation which is $N_g = 4$ in the present model. The RGEs for yukawa couplings $y_{1,2}$ in Eq.(9) are given by

$$(16\pi^2)\mu\frac{dy_1}{d\mu} = \left[-8g_3^2 + \frac{9}{2}y_1^2 + \frac{1}{2}y_2^2\right] y_1 , \tag{34}$$

$$(16\pi^2)\mu\frac{dy_2}{d\mu} = \left[-8g_3^2 + \frac{9}{2}y_2^2 + \frac{1}{2}y_1^2\right] y_2 , \tag{35}$$

and the RGEs for higgs quartic couplings $\lambda_{1,2,3,4}$ for the top-seesaw sector in Eq.(11) are given by [31, 37]

$$(16\pi^2)\mu\frac{d\lambda_1}{d\mu} = 24\lambda_1^2 + 2\lambda_3^2 + 2\lambda_3\lambda_4 + \lambda_4^2 + 12\lambda_1 y_1^2 - 6y_1^4 , \tag{36}$$

$$(16\pi^2)\mu\frac{d\lambda_2}{d\mu} = 24\lambda_2^2 + 2\lambda_3^2 + 2\lambda_3\lambda_4 + \lambda_4^2 + 12\lambda_2 y_2^2 - 6y_2^4 , \tag{37}$$

$$(16\pi^2)\mu\frac{d\lambda_3}{d\mu} = 2(\lambda_1 + \lambda_2)(6\lambda_3 + 2\lambda_4) + 4\lambda_3^2 + 2\lambda_4^2 + 6\lambda_3(y_1^2 + y_2^2) - 12y_1^2y_2^2 , \tag{38}$$

$$(16\pi^2)\mu\frac{d\lambda_4}{d\mu} = 4(\lambda_1 + \lambda_2)\lambda_4 + 4(2\lambda_3 + \lambda_4)\lambda_4 + 6\lambda_4(y_1^2 + y_2^2) + 12y_1^2y_2^2 . \tag{39}$$

The compositeness conditions in this model are given by [34, 35]

$$y_{1,2}^2(\mu) \to y_{1,2}^2(\Lambda) = \infty \tag{40}$$

$$\frac{\lambda_1(\mu)}{y_1^4(\mu)} \to \frac{\lambda_1(\Lambda)}{y_1^4(\Lambda)} = 0 \quad , \quad \frac{\lambda_2(\mu)}{y_2^4(\mu)} \to \frac{\lambda_2(\Lambda)}{y_2^4(\Lambda)} = 0, \tag{41}$$

$$\frac{\lambda_3(\mu)}{y_1^2(\mu)y_2^2(\mu)} \to \frac{\lambda_3(\Lambda)}{y_1^2(\Lambda)y_2^2(\Lambda)} = 0 \quad , \quad \frac{\lambda_4(\mu)}{y_1^2(\mu)y_2^2(\mu)} \to \frac{\lambda_4(\Lambda)}{y_1^2(\Lambda)y_2^2(\Lambda)} = 0 , \tag{42}$$

where Λ is called a compositeness scale and this scale is identified with the mass scale of the massive topcolor gluons $M_{G'}$ in the present model. The dynamics is then determined as follows: As a first step, we solve system of RGEs, Eqs.(33) -(39), under the compositeness conditions, Eqs.(40)-(42) for given Λ. As a second step, we find the physical solutions for $y_{1,2}$ and $\lambda_{1,2,3,4}$ from the on-shell conditions

$$\Sigma_D = \frac{v_1}{\sqrt{2}}\, y_1(\mu = \Sigma_D) \quad , \quad \Sigma_U = \frac{v_2}{\sqrt{2}}\, y_2(\mu = \Sigma_U)\,, \tag{43}$$

$$m_H = m_H(M_{\mathrm{TSS},0}, \lambda_1(m_H), \lambda_2(m_H), \lambda_3(m_H), \lambda_4(m_H))\,, \tag{44}$$

where $\Sigma_{U,D}$ is the dynamical fermion mass and m_H is the heavy CP-even higgs boson mass. In Fig.1, we show the results of solving the RGEs with the compositeness conditions for $\Lambda = 10, 50, 100\,$TeV. This corresponds to the first step described above.

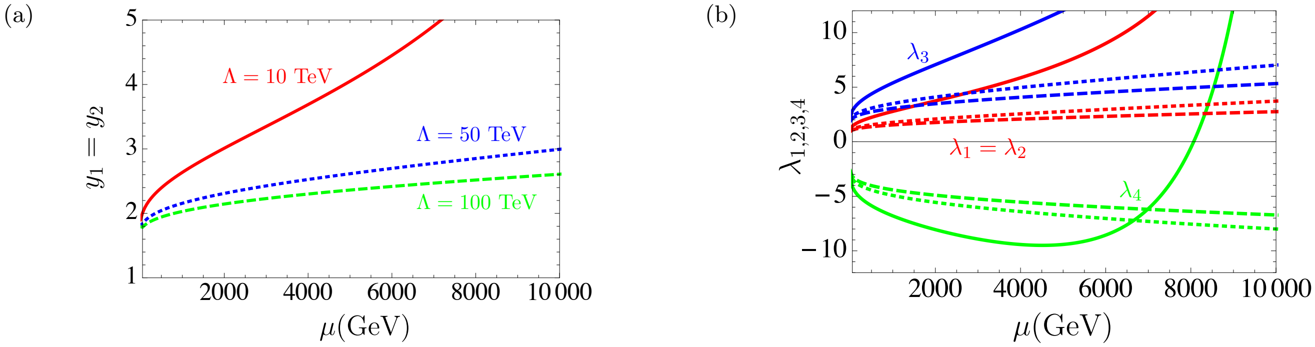

FIG. 1: The scale dependence of (a) yukawa couplings and (b) quartic couplings. In each panel, the solid, dotted and dashed lines correspond to $\Lambda = 10, 50$ and $100\,$TeV, respectively. In panel (b), the red curves correspond to $\lambda_1 = \lambda_2$, and blue and green curves correspond to λ_3 and λ_4, respectively.

We want to see if a light CP-even higgs with mass around $126\,$GeV can be accommodated within the model for arbitrary Λ with $\Lambda \geq 4\,$TeV which is satisfied with the lower bound $M_{G'} > 3.32\,$TeV at 95% C.L. from LHC [38]. First, we consider $M_{\mathrm{TSS},0} = 0$ in Eqs.(19) and (44), and $c_1 = c_2 = 0$ in Eq.(12). We solve the systems of RGEs, Eqs.(33) -(39) under the compositeness conditions, Eqs.(40) -(42) with the on-shell condition Eq.(44). In Fig. 2, we show the resultant m_h together with $m_h = 126\,$GeV line (horizontal cyan solid line) for $\tan\phi = 0.5, 1, 3$ and $\tan\beta = 0.5, 1, 3$. For nonzero and positive values of $M_{\mathrm{TSS},0}$, the scalar mass m_h should be below the $m_h = 126\,$GeV line, and we immediately find that the values $(\tan\phi, \tan\beta) = (0.5, 0.5), (0.5, 1), (1, 1)$ are disfavored for $m_h = 126\,$GeV.

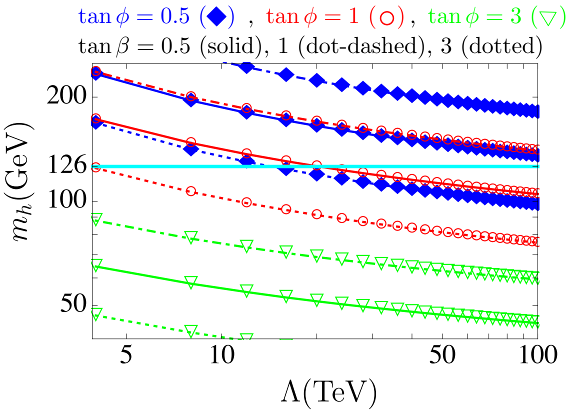

FIG. 2: The dynamical higgs mass in the top-seesaw sector for $4\,\mathrm{TeV} \leq \Lambda \leq 100\,\mathrm{TeV}$, i.e. m_h for Eq.(19) with $M_{\mathrm{TSS},0} = 0$. The horizontal cyan solid line shows $m_h = 126\,$GeV.

To constrain the allowed values of $(\tan\phi\,,\, \tan\beta)$ further, we consider the fermion masses. Since the top and bottom quark masses are sourced from ETC interactions as well as from the top-seesaw sector, we take them to be represented as

$$m_t \;=\; m_t(\mathrm{ETC}) + m_t(\mathrm{TSS}) = \epsilon_t m_t + (1-\epsilon_t) m_t\,, \tag{45}$$

$$m_b \;=\; m_b(\mathrm{ETC}) + m_b(\mathrm{TSS}) = \epsilon_b m_b + (1-\epsilon_b) m_b\,. \tag{46}$$

Here $m_{t,b}(\mathrm{ETC}) \equiv \epsilon_{t,b} m_{t,b}$ and $m_{t,b}(\mathrm{TSS}) \equiv (1-\epsilon_{t,b}) m_{t,b}$ correspond to the contributions to the top/bottom quark mass arising from the four fermion interactions due to the ETC sector and the top-seesaw sector, respectively. In the spirit of the original top-seesaw model, we require $0 \le \epsilon_t \le 0.5$ corresponding to $m_t(\mathrm{ETC}) \le m_t(\mathrm{TSS})$. To begin with, we fix

$$\epsilon_t = \epsilon_b = 0.5\,, \tag{47}$$

as representative values. In Fig. 3, we show the dynamical fermion mass $\Sigma_{U/D}$ for $4\,\mathrm{TeV} \le \Lambda \le 100\,\mathrm{TeV}$. In this figure, we take $\tan\phi = 0.5, 1, 3$ and $\tan\beta = 0.5, 1, 3$ as in Fig.2. In order to realize the top-seesaw dynamics, we must have $\Sigma_U > m_t(\mathrm{TSS}) = (1-\epsilon_t) m_t$ with $\epsilon_t = 0.5$. This limiting value of $m_t(\mathrm{TSS})$ in the case $\epsilon_t = 0.5$ is shown as the horizontal dotted line in the left panel of Fig.3. On the other hand, for the bottom sector, Σ_D is always larger than $m_b \simeq 4\,\mathrm{GeV}$, so no additional constraints arise here. Thus, combining Fig.2 and Fig.3, we take the benchmark values of $(\epsilon_t, \tan\phi, \tan\beta)$ as $\epsilon_t = 0.5$ and

$$\tan\phi = 1 \quad , \quad \tan\beta = 0.5\,, \tag{48}$$

$$\tan\phi = 1 \quad , \quad \tan\beta = 3\,, \tag{49}$$

$$\tan\phi = 0.5 \quad , \quad \tan\beta = 3\,, \tag{50}$$

$$\tan\phi = 3 \quad , \quad \tan\beta = 3\,. \tag{51}$$

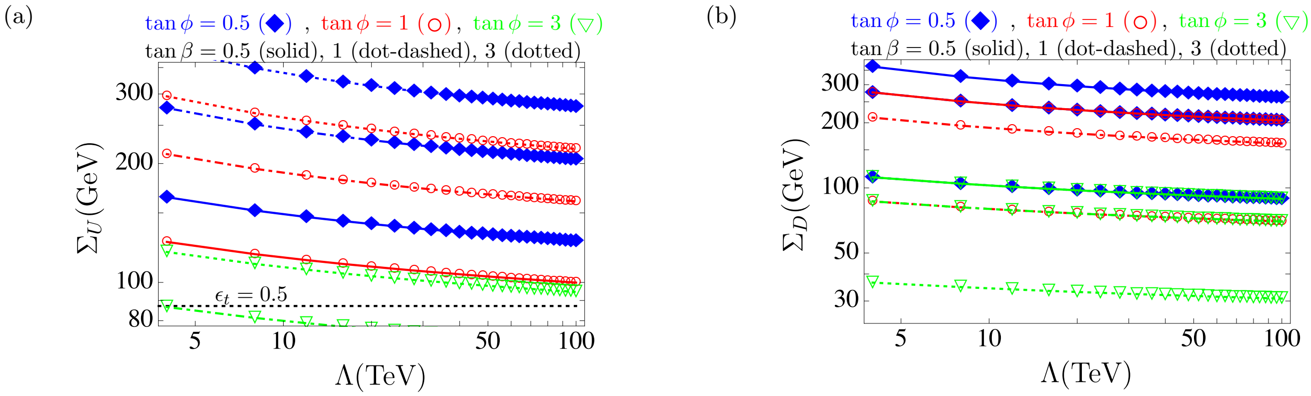

FIG. 3: The dynamical fermion mass for (a) top sector and (b) bottom sector with $\tan\phi = 0.5, 1, 3$ and $\tan\beta = 0.5, 1, 3$. The horizontal dotted line in (a) corresponds to $m_t(\mathrm{TSS}) = 0.5 m_t$.

We focus mainly on $\Lambda = 50\,\mathrm{TeV}$, which also diminishes the contributions from the massive topcolor gauge bosons to the electroweak precision parameters [24, 26]. To fix the parameter $M_{\mathrm{TSS},0}$, we consider the benchmark parameter values listed above, $\epsilon_t = 0.5$ and $\Lambda = 50\,\mathrm{TeV}$. For each of these parameter sets, in Fig. 4, we show (a) the CP-even higgs boson masses and (b) their mixing angles. From Fig. 4(a), we find that for the lighter state, h, the value $m_h = 126\,\mathrm{GeV}$ can be realized if $M_{\mathrm{TSS},0} \simeq 100\,\mathrm{GeV}$ for cases in Eqs.(48,49,50) or $M_{\mathrm{TSS},0} \simeq 1\,\mathrm{TeV}$ for the case in Eq.(51). For the case of Eq.(51), corresponding to the dot-dashed curves in Fig.4(a), it is also possible to have the heavier state, H, to satisfy $m_H = 126\,\mathrm{GeV}$ for $M_{\mathrm{TSS},0} \simeq 70\,\mathrm{GeV}$. We will return to this special case shortly, but consider first the case of the lighter state h satisfying $m_h = 126\,\mathrm{GeV}$. In Fig.4(b), the horizontal solid line is $\cos\alpha = 1/\sqrt{2}$, and above (below) this line $|\tan\alpha| < 1$ ($|\tan\alpha| > 1$). Based on Fig. 4 and the discussion below Eq. (22), we expect that the state h with mass of 126 GeV originates mainly from the condensate $\langle \overline{U}_L^{(3)} U_R^{(4)} \rangle \neq 0$ in the case of Eqs. (48) and (51). On the other hand, in the case of Eqs. (49) and (50) the state h, and in the case of Eq. (51) the state H, come mainly from $\langle \overline{D}_L^{(3)} D_R^{(4)} \rangle \neq 0$. Therefore, in order to realize $m_{h,H} = 126\,\mathrm{GeV}$ at $\Lambda = 50\,\mathrm{TeV}$

we take

$$M_{\mathrm{TSS},0} = 77\,\mathrm{GeV} \quad \text{for} \quad \tan\phi = 1 \quad , \quad \tan\beta = 0.5\,, \tag{52}$$

$$M_{\mathrm{TSS},0} = 111\,\mathrm{GeV} \quad \text{for} \quad \tan\phi = 1 \quad , \quad \tan\beta = 3\,, \tag{53}$$

$$M_{\mathrm{TSS},0} = 78\,\mathrm{GeV} \quad \text{for} \quad \tan\phi = 0.5 \quad , \quad \tan\beta = 3\,. \tag{54}$$

$$M_{\mathrm{TSS},0} = 960\,\mathrm{GeV} \quad \text{for} \quad \tan\phi = 3 \quad , \quad \tan\beta = 3\,, \tag{55}$$

for $m_h = 126\,\mathrm{GeV}$ and

$$M_{\mathrm{TSS},0} = 73\,\mathrm{GeV} \quad \text{for} \quad \tan\phi = 3 \quad , \quad \tan\beta = 3\,, \tag{56}$$

for $m_H = 126\,\mathrm{GeV}$.

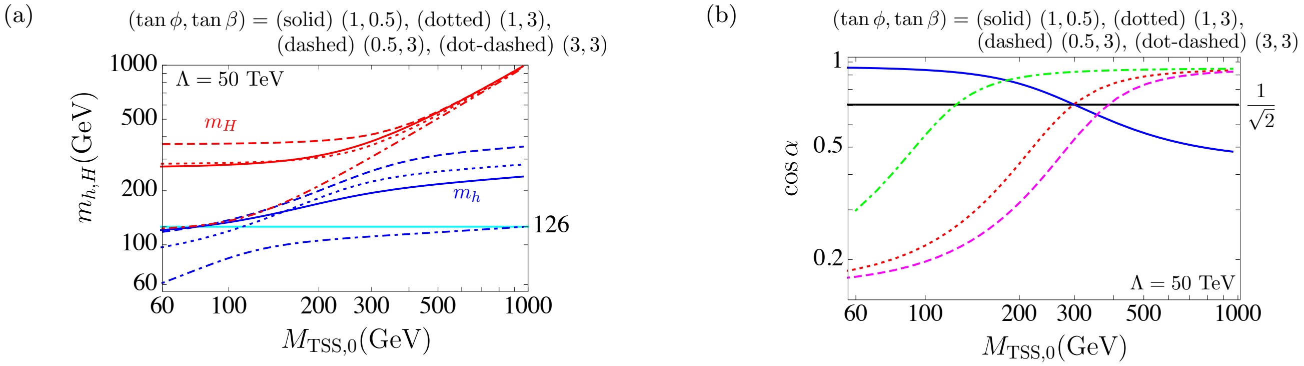

FIG. 4: (a) The CP-even higgs boson masses and (b) the mixing angles (α in Eq.(20)) between two CP-even higgs bosons at $\Lambda = 50\,\mathrm{TeV}$ with varying $M_{\mathrm{TSS},0}$. In both panels, each curve corresponds to $(\tan\phi\,,\,\tan\beta)$ = (solid) $(1, 0.5)$, (dotted) $(1, 3)$, (dashed) $(0.5, 3)$ and (dot-dashed) $(3, 3)$. The horizontal cyan solid line shows (a) $m_h = 126\,\mathrm{GeV}$ and (b) $\alpha = \pi/4$, i.e. $|\cos\alpha| = |\sin\alpha|$.

Based on the benchmark parameters, Eqs. (48)-(51), we next discuss the quark mixing angles. First, the fermion mass part after the dynamical electroweak symmetry breaking is

$$-\begin{pmatrix}\bar{U}_L^{(3)} & \bar{U}_L^{(4)}\end{pmatrix}\begin{pmatrix}0 & \Sigma_U \\ M_U^{(43)} & M_U^{(44)}\end{pmatrix}\begin{pmatrix}U_R^{(3)} \\ U_R^{(4)}\end{pmatrix} - \begin{pmatrix}\bar{D}_L^{(3)} & \bar{D}_L^{(4)}\end{pmatrix}\begin{pmatrix}0 & \Sigma_D \\ M_D^{(43)} & M_D^{(44)}\end{pmatrix}\begin{pmatrix}D_R^{(3)} \\ D_R^{(4)}\end{pmatrix} + \mathrm{h.c.}\,, \tag{57}$$

where $M_{U,D}^{(43,44)}$ are the mass parameters which do not contribute to the dynamical electroweak symmetry breaking, and they are arbitrary parameters in the present model framework. Now, we assume that the quark mixing matrices U, D reflect the seesaw mechanism for the third generation and their vector-like partners, and hence the quark mixing matrices are written as

$$U^L_{\alpha\beta} \simeq \begin{pmatrix}1 & 0 & 0 & 0 \\ 0 & 1 & 0 & 0 \\ 0 & 0 & c^t_L & s^t_L \\ 0 & 0 & -s^t_L & c^t_L\end{pmatrix} \quad , \quad U^R_{\alpha\beta} \simeq \begin{pmatrix}1 & 0 & 0 & 0 \\ 0 & 1 & 0 & 0 \\ 0 & 0 & -c^t_R & s^t_R \\ 0 & 0 & s^t_R & c^t_R\end{pmatrix}\,, \tag{58}$$

$$D^L_{\alpha\beta} = U^L_{\alpha\beta}\,|_{t\to b} \quad , \quad D^R_{\alpha\beta} = U^R_{\alpha\beta}\,|_{t\to b}\,. \tag{59}$$

where $c^t_L \equiv \cos\theta^t_L$, $s^t_R \equiv \sin\theta^t_R$, etc. These fermion mixing matrices, U and D in Eqs.(58) and (59), diagonalize the mass matrices in Eq.(57), and the eigenvalues are identified with $m_{t,b}(\mathrm{TSS})$ and $m_{T,B}$ where $m_{T,B}$ ($> m_{t,b}(\mathrm{TSS})$) is mass of the vector-like partner of the third generation quark. Therefore $c^{t,b}_L, s^{t,b}_R$ should satisfy

$$[c^t_L]^2 \equiv \frac{m_T^2 - \Sigma_U^2}{m_T^2 - m_t^2(\mathrm{TSS})} \quad , \quad [s^t_R]^2 \equiv \frac{m_t^2(\mathrm{TSS})}{\Sigma_U^2}[c^t_L]^2\,, \tag{60}$$

$$[c^b_L]^2 \equiv \frac{m_B^2 - \Sigma_D^2}{m_B^2 - m_b^2(\mathrm{TSS})} \quad , \quad [s^b_R]^2 \equiv \frac{m_b^2(\mathrm{TSS})}{\Sigma_D^2}[c^b_L]^2\,. \tag{61}$$

Thus the fermion mixing angles are determined by the solutions to the RGEs, compositeness conditions and on-shell conditions in Eqs.(60) and (61) for arbitrary values of $m_{T,B}$. In Fig.5, we show the resultant $c_L^t, s_R^t, c_L^b, s_R^b$ for the benchmark parameters given in Eqs.(48)-(51). Within each $(\tan\phi\,,\,\tan\beta)$-group we consider values $m_{T,B} = 0.8, 1, 2, 5\,\mathrm{TeV}$. The horizontal dot-dashed line in (c-1,2) is the 95% C.L. allowed line by the constraint for $\delta g_L^b = (1/2)(s_L^b)^2$. This correction to g_L^b arises at tree level in the present model (for details, see section IV B), and the allowed region is above this line. In order that fermion sector does not generate a large contribution to the T-parameter, we set

$$m_T = m_B = 5\,\mathrm{TeV}\,. \tag{62}$$

Since Eq.(61) implies $[c_L^b]^2 \simeq 1-(\Sigma_D/m_B)^2$, i.e. $[s_L^b]^2 \simeq (\Sigma_D/m_B)^2$ for $m_B \gg m_b(\mathrm{TSS})$, we see that the above choice for m_B is also not affected by the δg_L^b constraint; see Fig.5(c-1,2).

To finish this section, in Fig.6 we show the higgs boson mass corresponding to different points in the parameter space of the model: (a) Eq.(52), (b) Eq.(53), (c) Eq.(54) and (d) Eq.(55). The mass of the vectorlike B quarks is given in Eq. (62). Of course these results depend on values of (c_1, c_2), and we consider values (c_1, c_2) which minimize the T-parameter as will be shown in the section IV A. For the case (d), the dependence of the results on (c_1, c_2) is small. In Fig. 6, the blue solid curves correspond to m_h, blue dotted curves to m_H, red solid curves to m_{A_1}, red dotted curves to m_{A_2}, green solid curves to $m_{H_1^\pm}$ and green dotted curves to $m_{H_2^\pm}$. In all panels, m_{A_2} and $m_{H_2^\pm}$ have almost degenerate mass around $m^2_{\mathrm{ETC}} = \Lambda^2_{\mathrm{TC}} = 4\pi v^2_{\mathrm{TC}}$ of Eq. (32). In the case of parameter values in (d), corresponding to $(\tan\phi, \tan\beta) = (3, 3)$, we find hierarchical structure of the higgs boson masses as $m_h \simeq 126\,\mathrm{GeV} < m_H \simeq m_{A_1} \simeq m_{H_1^\pm} < m_{A_2}, m_{H_2^\pm}$. On the other hand, in the case of (a), (b) and (c) parameter values, corresponding to $(\tan\phi, \tan\beta) = (1, 0.5), (1, 3), (0.5, 3)$, we find the hierarchical structure $m_h, m_{A_1} \simeq 126\,\mathrm{GeV} < m_H \simeq m_{H_1^\pm} < m_{A_2}, m_{H_2^\pm}$. Now, focus on the case of Eq.(56), i.e. $m_H = 126\,\mathrm{GeV}$ at $\Lambda = 50\,\mathrm{TeV}$. In this case the charged higgs boson is light, with a mass $m_{H_1^\pm} \simeq m_H = 126\,\mathrm{GeV}$, i.e. $m_{H_1^\pm} < m_t$. In the present model this charged higgs is analogous with the charged top pion in the topcolor model. From [9], the light charged higgs with $m_{H^\pm} \simeq 130\,\mathrm{GeV}$ is ruled out for $\sin\omega \simeq 0.3$ where the parameter $\sin\omega$ of [9] corresponds to v_2/v_{EW} in the present model. For $(\tan\phi, \tan\beta) = (3, 3)$, we have $v_2/v_{\mathrm{EW}} = 0.3$, and we conclude that $m_{H_1^\pm} \simeq 130\,\mathrm{GeV}$ is ruled out by the charged higgs boson search and thus we eliminate the representative point, Eq.(56), and will not consider it further in this paper.

IV. EWPT AND δg_L^b CONSTRAINTS

In this section we shall constrain the representative points, Eqs.(52)-(55) from the electroweak precision tests (EWPT) and δg_L^b including the one-loop corrections.

A. EWPT parameter for the higgs sector in the present modell

In this section, we consider the EWPT constraints in the present model. By using Eq.(8) in the mass basis of PNGBs and higgses, we obtain the Feynman rules in Tables. II,III and IV in appendix A. Then we compute higgs contributions to the vacuum polarization at the one loop as shown in Fig.7. The results for the Peskin-Takeuchi S and T parameters [39] are given in appendix A. The results are similar to the generic three higgs doublet model. The difference arises from the fact that since we treat the TC sector using the non-linear sigma model, one of the higgs doublets does not contain the CP-even higgs boson; see Eq.(5). This leads to non-cancelling $1/\epsilon$-contribution in the S and T parameters. However, this is not a problem, but merely reflects that our effective model is not ultraviolet complete theory, but should be only studied below a finite cutoff scale. Therefore, to interpret the final results in terms of the cutoff of effective theory, we replace these divergent part as

$$\frac{1}{\epsilon} + 1 \to \ln \Lambda^2_{\mathrm{TC}}\,, \tag{63}$$

where Λ_{TC} is the cutoff of the effective theory for the TC sector and we take $\Lambda_{\mathrm{TC}} = 4\pi v_{\mathrm{TC}}$.

In Fig.8 we show the EWPT constraint for the present model with the representative points of the parameters as given in Eqs.(52), (53) and (55) with $m_T = m_B = 5\,\mathrm{TeV}$, $\Lambda = 50\,\mathrm{TeV}$ and varying (c_1, c_2) in the range $0.1 \le c_{1,2} \le 5$. We focus on this range, since for $c_{1,2} > 5$, the values of T become large, around $T > 0.4$. The shaded regions corresponds to $68, 95, 99\%$ C.L. allowed region from inner to outer ellipses, and experimental results of S, T are [40]

$$S = 0.04 \pm 0.09 \quad , \quad T = 0.07 \pm 0.08\,, \tag{64}$$

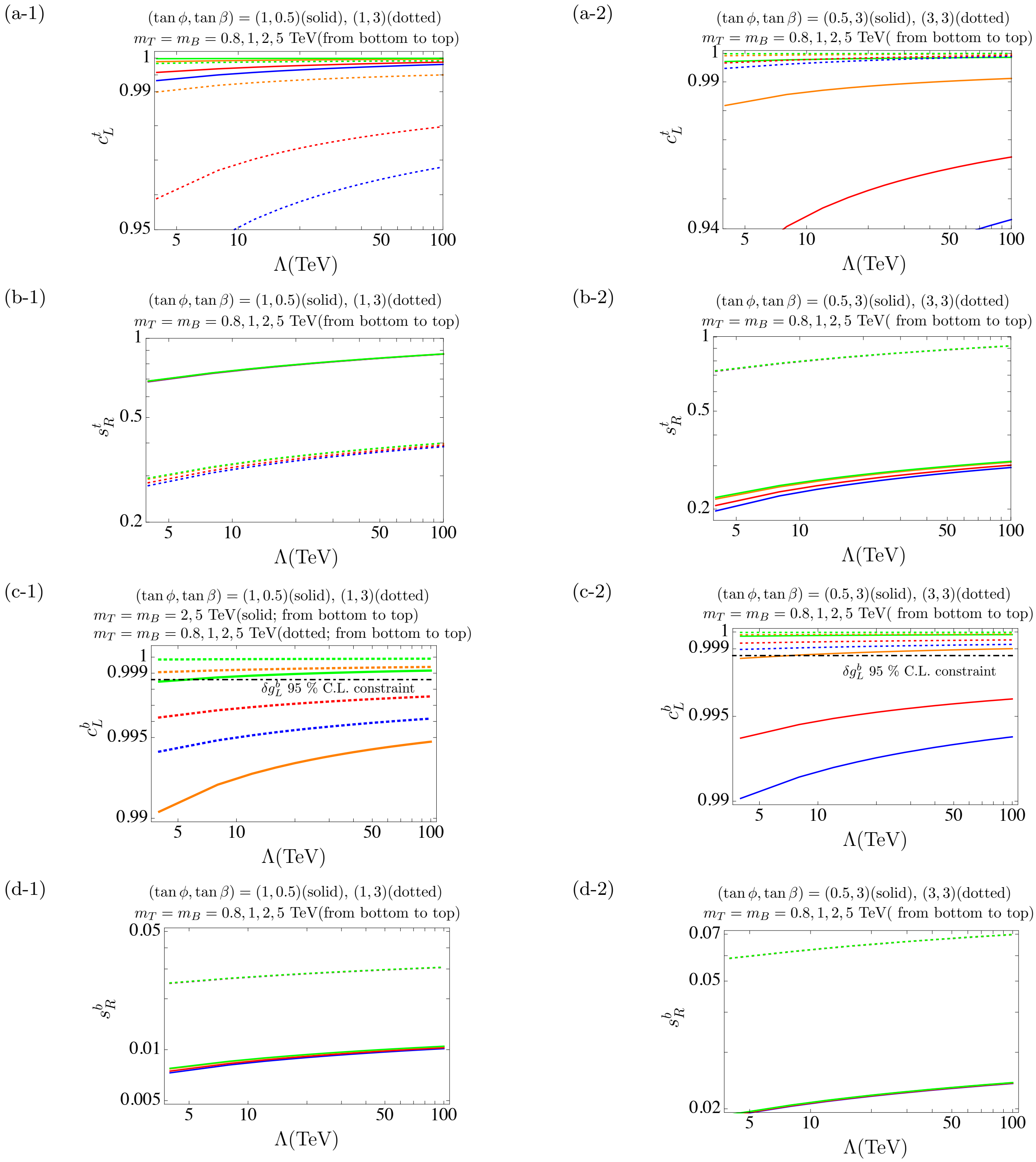

FIG. 5: The mixing angles of fermions. The panels (a,b,c,d-1) correspond to $(\tan\phi\,,\,\tan\beta) =$ (solid curves) $(1, 0.5)$ and (dotted curves) $(1, 3)$, and (a,b,c,d-2) correspond to $(\tan\phi\,,\,\tan\beta) =$ (solid curves) $(0.5, 3)$ and (dotted curves) $(3, 3)$. In all panels, $m_{T,B} = 800\,\text{GeV}, 1, 2, 5\,\text{TeV}$ from bottom curves to top curves (blue,red,orange,green) in the same $(\tan\phi\,,\,\tan\beta)$-groups. The horizontal magenta dot-dashed line in (c-1,2) shows the 95% C.L. allowed line by the constraint for δg_L^b (see section.IV B).

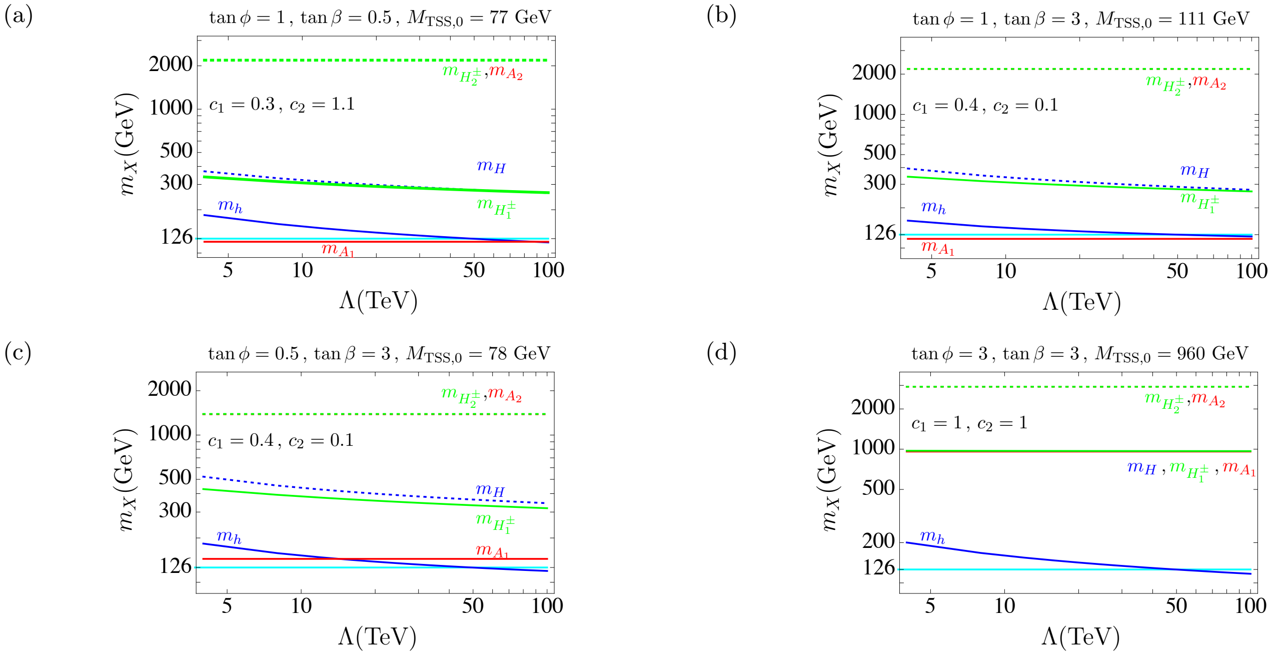

FIG. 6: Higgs boson mass in the top-seesaw assisted walking TC model for $4\,\text{TeV} \leq \Lambda \leq 100\,\text{TeV}$. Each panel corresponds to $(\tan\phi, \tan\beta, c_1, c_2) =$ (a) $(1, 0.5, 2, 0.1)$, (b) $(1, 3, 0.1, 0.1)$, (c) $(0.5, 3, 0.1, 0.1)$ and (d) $(3, 3, 1, 1)$. $m_{h,H,A_1,A_2,H_1^\pm,H_2^\pm}$ are blue solid, blue dotted, red solid, red dotted, orange solid, orange dotted curves, respectively.The horizontal cyan solid line shows $m_h = 126\,\text{GeV}$ in all panels.

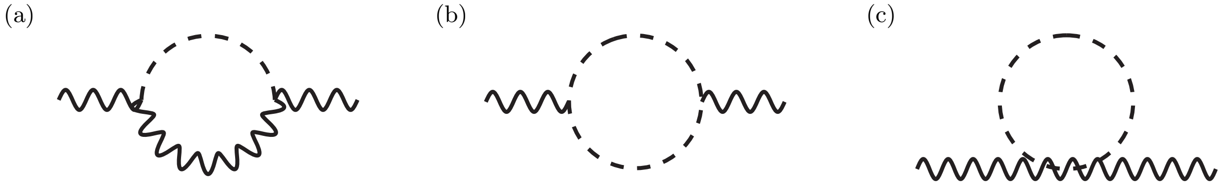

FIG. 7: The higgs/NGBs contribution to the vacuum polarization. The dashed line and wave line correspond to higgs/NGBs and gauge boson, respectively.

and these central values are presented by the cross in Fig.8. We take the reference higgs boson mass as $m_h^{\rm ref} = 117\,\text{GeV}$. The results are insensitive if this reference value is varied in a range $115.5\,\text{GeV} < m_h^{\rm ref} < 127\,\text{GeV}$ as in [40]. So far our discussion of the technicolor sector has been general. For illustration, here we also consider how the more detailed features may affect the results. As an example, consider minimal walking technicolor, where a fourth chiral generation of leptons arises due to cancellation of a global anomaly. Hence, in the present model, S and T are given by

$$S = S_{\rm TC} + S_{\rm 3HDM} + S_{N,E} + S_{q4} + S_{G',Z'} + \Delta_S\,, \tag{65}$$

$$T = T_{\rm TC} + T_{\rm 3HDM} + S_{N,E} + T_{q4} + T_{G',Z'} + \Delta_T\,, \tag{66}$$

The factors with subscript TC correspond to the contribution from the TC sector and will be discussed below. The factors with subscript 3HDM correspond to the contributions from the three Higgs doublet sector, and are given in Eqs.(A1) and (A2). The factors with subscript N, E and $q4$ and G', Z' correspond to the contribution from the fourth generation chiral leptons, vectorlike quarks and heavy topcolor gauge bosons, respectively, and these are explicitly given in [26]. Note that the contribution from new chiral leptons arises only if we associate the technicolor sector with minimal walking technicolor. The contributions $S_{G',Z'}$ and $T_{G',Z'}$ become large below $\Lambda \simeq 10\,\text{TeV}$ but are small and negligible for $\Lambda \geq 50\,\text{TeV}$. Since we concentrate on $\Lambda \simeq 50\,\text{TeV}$, we do not consider these contributions. Finally, the factors $\Delta_{S,T}$ contain the contributions from the SM-like CP-even scalar h^0, and the subtraction of the SM higgs contribution; see [26].

We assume that the TC sector conserves custodial symmetry, and hence we take $T_{\rm TC} = 0$. For the TC contributions to the S-parameter, we consider the generic TC sector without extra leptons, i.e. (i) $S_{\rm TC} = 0$, $S_{E,N} = T_{E,N} = 0$, and TC sector of minimal walking technicolor (ii) $S_{\rm TC} = 0$ with $(m_N, m_E) = (120\,{\rm GeV}, 100\,{\rm GeV})$, (iii) $S_{\rm TC} = 0.1$ with $(m_N, m_E) = (120\,{\rm GeV}, 100\,{\rm GeV})$. These correspond to groups (i),(ii),(iii) in Fig.8, respectively. From Fig.8, we find that the EWPT constraint allow $(\tan\phi\,, \tan\beta) = (1, 0.5), (3, 3)$ among the present representative values in Eqs.(52,53,54,55). In the case of $(\tan\phi\,, \tan\beta) = (1, 3), (0.5, 3)$, the minimum values of T are given $T \simeq 0.31, 0.6$, respectively. The origin of these rather large values can be traced to the spectrum: From Fig.6 (b) and (c), corresponding to $(\tan\phi\,, \tan\beta) = (1, 3), (0.5, 3)$, we find $m_{A_1} < m_{H,H_1^\pm}$ and this splitting causes a large contribution to T-parameter similarly with the top-seesaw model [24]. From Fig.6 (a), corresponding to $(\tan\phi\,, \tan\beta) = (1, 0.5)$, we also find $m_{A_1} < m_{H,H_1^\pm}$ but in this case $m_{A_1} \simeq m_h$ at around $\Lambda = 50\,{\rm TeV}$, so in this case the overall contribution to T-parameter remains smaller, and the result can remain within the $S - T$ ellipsis in Fig.8. The above results are not affected by variation of ϵ_b, since the fermion contribution to S, T- parameters do not depend on s_R^b and the dependence of c_L^b on ϵ_b is negligibly small.

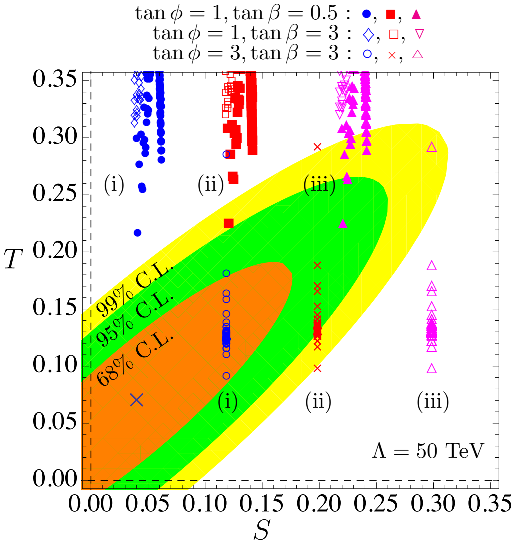

FIG. 8: The EWPT constraint for $(\tan\phi\,, \tan\beta) = (1, 0.5), (1, 3), (3, 3)$ with $m_T = m_B = 5\,{\rm TeV}$ and $\Lambda = 50\,{\rm TeV}$. A case of $(\tan\phi\,, \tan\beta) = (0.5, 3)$ is on $T \geq 0.6$. We vary c_1, c_2 in a range $[0.1, 5]$. Groups (i),(ii),(iii) correspond to $S_{\rm TC} = 0$, $S_{\rm TC} = 0$ with $(m_N, m_E) = (120\,{\rm GeV}, 100\,{\rm GeV})$, $S_{\rm TC} = 0.1$ with $(m_N, m_E) = (120\,{\rm GeV}, 100\,{\rm GeV})$, respectively. The shaded region corresponds to $68, 95, 99\%$ C.L. allowed region from inner to outer. × shows $S = 0.04\,, T = 0.07$.

B. $Z\bar{b}_L b_L$ constraint

Generally, light charged higgs bosons with mass around 300 GeV are constrained by the experimental value of R_b and A_b; for the case of 2HDM, see [41]. In this section, we discuss the radiative correction to δg_L^b, which is defined as

$$\frac{g}{c_W} Z_\mu \bar{b}_L [g_L^b + \delta g_L^b] b_L\,, \tag{67}$$

for the higgs sector in the present model. Now, the interactions between fermions and electroweak gauge bosons in the fermion mass basis are given by

$$\mathcal{L}_{Vff} = \frac{2}{3} e A_\mu \left[\bar{t}\gamma^\mu t + \bar{T}\gamma^\mu T\right] - \frac{1}{3} e A_\mu \left[\bar{b}\gamma^\mu b + \bar{B}\gamma^\mu B\right] + \left[Z\bar{f}f + W\bar{f}f \text{ terms}\right]\,, \tag{68}$$

where $\left[Z\bar{f}f + W\bar{f}f \text{ terms}\right]$ are given in Table V in appendix A and $g_{L,R}^{t,b}$ is given by

$$g_L^t = \frac{1}{2} - \frac{2}{3} s_W^2 \quad , \quad g_R^t = -\frac{2}{3} s_W^2\,, \tag{69}$$

$$g_L^b = -\frac{1}{2} + \frac{1}{3} s_W^2 \quad , \quad g_R^b = \frac{1}{3} s_W^2\,. \tag{70}$$

For our analysis, we also need the yukawa interactions among 2+1 higgs doublets and fermions. In the present model, the yukawa terms for third generation quarks and their vector-like partners, which is a part of Eq.(9), are

$$\mathcal{L}^{3-4}_{\rm yukawa} = -y_1 \bar{Q}^{(3)}_L \Phi_1 D^{(4)}_R - y_2 \bar{Q}^{(3)}_L \tilde{\Phi}_2 U^{(4)}_R - y^b_{\rm TC} \bar{q}_L \Phi_{\rm TC} b_R - y^t_{\rm TC} \bar{q}_L \tilde{\Phi}_{\rm TC} t_R + \text{h.c.}\,, \tag{71}$$

where the first and second terms are written in the topcolor interaction basis for fermions but the third and fourth terms are in the mass basis for fermions. The couplings $y_{1,2}$ are solved from RGEs, Eqs.(33)-(39) under the compositeness conditions, Eqs.(40)-(42) with on-shell condition Eqs.(43). On the other hand, the couplings $y^{b,t}_{\rm TC}$ are given by

$$y^b_{\rm TC} = \frac{\sqrt{2}\epsilon_b m_b}{v_{\rm TC}} \quad , \quad y^t_{\rm TC} = \frac{\sqrt{2}\epsilon_t m_t}{v_{\rm TC}}\,, \tag{72}$$

where $\epsilon_{t,b}$ are defined in Eqs. (45) and (46). For our purpose, it is enough to consider yukawa interactions which include the charged scalar particles and the left-handed bottom quark, and these yukawa interactions are given in Table VI in appendix A. The experimental 95% C.L. constraint for $[\delta g^b_L]$ by both R_b and A_b is given by [42]

$$-2.7 \times 10^{-3} \leq \delta g^b_L \leq 1.4 \times 10^{-3} \quad (95\%\,\text{C.L.})\,. \tag{73}$$

Throughout the calculation in this section, we will work under the assumption $m_b^2 = 0$.

In the present model, one can see easily from Table V that δg^b_L at the tree level is given by

$$[\delta g^b_L]_{\rm tree} = \frac{1}{2}(s^b_L)^2\,. \tag{74}$$

As to the one-loop radiative correction, we divide it into two parts: one including the EW gauge boson in the loop, and another that does not include any EW gauge bosons. We denote these two corrections as $[\delta g^b_L]^{\rm 1loop}_{\rm gauge}$ and $[\delta g^b_L]^{\rm 1loop}_{\rm NGB}$, respectively. Diagrammatically, $[\delta g^b_L]^{\rm 1loop}_{\rm gauge}$ is

$$[\delta g^b_L]^{\rm 1loop}_{\rm gauge} =$$

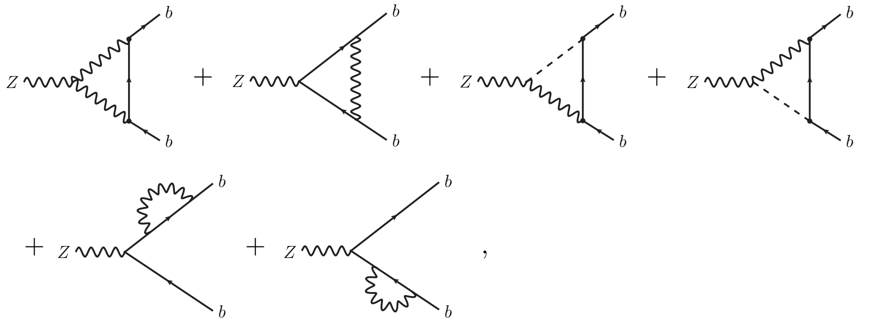

(75)

and $[\delta g^b_L]^{\rm 1loop}_{\rm NGB}$ is

$$[\delta g^b_L]^{\rm 1loop}_{\rm NGB} =$$

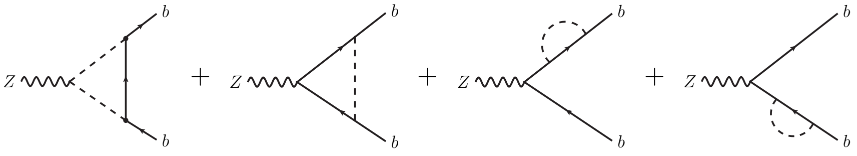

(76)

We take the incoming Z boson momentum equal to zero. Using the results from Appendix A, we obtain the renormalized $[\delta g^b_L]^{\rm 1loop}$ as follows: First, the UV-divergences are renormalized as [43]

$$[\delta g^b_L]^{\rm 1loop}_{\rm reno.} \equiv [\delta g^b_L]^{\rm 1loop} - [\delta g^b_L]^{\rm 1loop}_{m_t^2, m_T^2 = 0}\,. \tag{77}$$

Thus the deviation from g^b_L in the SM in the present model is given by

$$[\delta g^b_L] = [\delta g^b_L]_{\rm tree} + \Delta[\delta g^b_L]^{\rm 1loop}. \tag{78}$$

Here $\Delta[\delta g^b_L]^{\rm 1loop}$ is defined as

$$\Delta[\delta g^b_L]^{\rm 1loop} \equiv [\delta g^b_L]^{\rm 1loop}_{\rm reno.} - [\delta g^b_L]^{\rm SM-1loop}_{\rm reno.}\,, \tag{79}$$

and $[\delta g_L^b]^{\rm SM-1loop}_{\rm reno.}$ is given by $[\delta g_L^b]^{\rm 1loop}_{\rm reno.}$ in the limit $\cos\theta_L^{t,b} \to 1\,, \Sigma_U \to 0\,, \cos\phi \to 0\,, \epsilon_t \to 1\,, v_{\rm TC} \to v_{\rm EW}$. Let us perform a nontrivial check on our results by taking a limit $c_L^b \to 1$, $s_R^{t,b} \to 1$, $\tan\zeta \to \infty$ and $\tan\beta \to \infty$ with $1 - \epsilon_t \gg \epsilon_t$. This corresponds to the well-known TC2 model [44]. In this limit, $[\delta g_L^b]_{\rm gauge}$ in Eq.(A12) reduces to the SM one-loop result, but $[\delta g_L^b]_{\rm NGB}$ in Eq.(A13) contains also a contribution beyond the Standard Model. Thus under this limit, we find a result

$$\begin{aligned}[\delta g_L^b]_{\rm TC2} &= -\frac{1}{2}\frac{1}{16\pi^2}[Y_{tb}^G]^2 C_{01}(m_t^2, M_W^2)\,, \\ &= \frac{1}{2}\frac{1}{16\pi^2}\left[\frac{\sqrt{2}m_t}{v_2}\frac{v_{\rm TC}}{v_{\rm EW}}\right]^2 \left(-\frac{x}{(x-1)^2}\ln x + \frac{x}{x-1}\right)\,, \end{aligned} \tag{80}$$

where $x \equiv m_t^2/M^2_{H_2^\pm}$, and this result reproduces the result obtained in [45].

Turning to our model study, then, in Fig.9, we show constraint for $[\delta g_L^b]$ defined as Eq.(78) with parameter values from Eqs.(52)and (55), which are allowed by the EWPT constraint as seen from Fig.8. The shaded region shows the 95% C.L. allowed region in accordance with Eq.(73). In Table I, we summarize the judgement of the experimental constraints we have considered for the representative parameter values from Eqs.(48)-(51) and Eqs.(52-(55). Thus, among the representative values Eqs.(52)-(55) the EWPT and δg_L^b constraints favor only a case of

$$\tan\phi = 3 \quad , \quad \tan\beta = 3 \quad \text{with} \quad M_{\rm TSS,0} = 960\,{\rm GeV}\,, \tag{81}$$

which derives $m_h = 126\,{\rm GeV}$ at $\Lambda = 50\,{\rm TeV}$, and this light CP-even higgs boson arises mainly from $\langle \bar{U}_L^{(3)} U_R^{(4)} \rangle \neq 0$ since $|\tan\alpha| < 1$ as shown in Fig.4(b). The results are insensitive to variations of ϵ_b since $[\delta g_L^b]$ does not depend on s_R^b, and the dependence of c_L^b on ϵ_b is negligibly small.

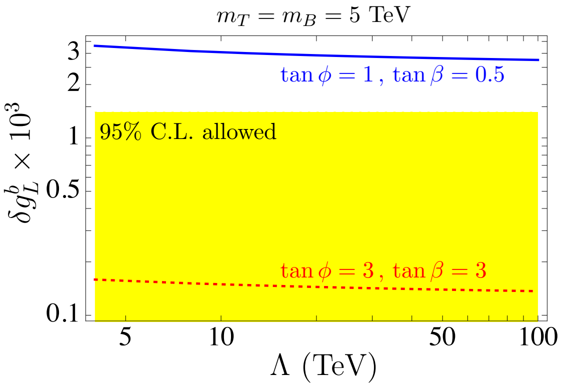

FIG. 9: δg_L^b constraint for the present model for $(\tan\phi\,, \tan\beta)$ = (solid) $(1, 0.5)$ and (dotted) $(3, 3)$ with $m_T = m_B = 5\,{\rm TeV}$. The shaded region shows the 95% C.L. allowed region in accordance with Eq.(73).

$\tan\phi$	$\tan\beta$	$M_{\rm TSS,0}$	at $\Lambda = 50\,{\rm TeV}$	$m_{H_1^\pm} > m_t$	EWPT (Fig.8)	δg_L^b (Fig.9)
1	0.5	77 GeV	$m_h = 126\,{\rm GeV}$	Yes	Yes (4th leptons are necessary)	No
1	3	111 GeV	$m_h = 126\,{\rm GeV}$	Yes	No	-
0.5	3	78 GeV	$m_h = 126\,{\rm GeV}$	Yes	No	-
3	3	73 GeV	$m_H = 126\,{\rm GeV}$	No	-	-
3	3	960 GeV	$m_h = 126\,{\rm GeV}$	Yes	Yes (4th leptons are not necessary)	Yes

TABLE I: Summary of the representative values of $(\tan\phi\,, \tan\beta)$ in Eqs.(48,49,50,51). "Yes" means allowed by the constraint and "No" means not allowed by the constraint. The hyphen ("-") means that this is not needed. As to $m_{H_1^\pm}$ constraint, see section III.

V. THE MODEL AND 126 GeV HIGGS AT THE LHC

In this section, we focus on the light CP-even higgs boson h^0 in the present model, and compare the present model with the recent LHC higgs search results for the representative values

$$\tan\phi = 3 \quad , \quad \tan\beta = 3 \quad \text{with} \quad M_{\text{TSS},0} = 960\,\text{GeV} \quad \text{and} \quad m_T = m_B = 5\,\text{TeV}\,. \tag{82}$$

In this section we fix $\epsilon_t = 0.5$ but we vary ϵ_b in a range $0.1 \le \epsilon_b \le 1$ which does not affect the experimental constraints discussed in section IV. For the LHC phenomenology, the relevant part of the full Lagrangian is

$$\begin{aligned}
\mathcal{L} = {} & C_{hWW}\left(gM_W \cdot W_\mu^+ W^{-\mu} + \frac{g}{2c_W} M_Z \cdot Z_\mu Z^\mu\right) h \\
& - C_{hff}\frac{m_f}{v_{\text{EW}}} \cdot h\bar{f}f - h\left[C^L_{hFf}\bar{F}_R f_L + C^L_{hfF}\bar{f}_R F_L + C^R_{hFf}\bar{F}_L f_R + C^R_{hfF}\bar{f}_L F_R\right] \\
& + C_{Wff}\frac{g}{\sqrt{2}}\left[\bar{f}^u_{iL}\gamma^\mu W^+_\mu V_{ij} f^d_{jL} + \text{h.c.}\right] \\
& + \frac{g}{2c_W} Z_\mu \bar{f}\gamma^\mu\left[C^V_{Zff}\hat{v}_f - C^A_{Zff}\hat{a}_f\gamma_5\right] f + \frac{g}{c_W} Z_\mu \sum_{F\neq f} \bar{F}\gamma^\mu \left[C^L_{ZFf}\frac{1-\gamma_5}{2} + C^R_{ZFf}\frac{1+\gamma_5}{2}\right] f \\
& + (gM_W)\sum_{i=1,2} C_{hH_i^\pm H_i^\pm}\phi H_i^+ H_i^- + \frac{ig(c_W^2 - s_W^2)}{2c_W} Z_\mu \sum_{i=1,2}\left[(\partial^\mu H_i^+)H_i^- - H_i^+(\partial^\mu H_i^-)\right] ,
\end{aligned} \tag{83}$$

where V_{ij} is the CKM (MNS) matrix if $f_i^{u,d}$ are quarks(leptons) and $\hat{v}_f, \hat{a}_f$ are defined as

$$\hat{v}_f = g_L^f + g_R^f = T_3^f - 2s_W^2 Q_f\,, \tag{84}$$

$$\hat{a}_f = g_L^f + g_R^f = T_3^f\,. \tag{85}$$

In the SM case, prefactors C in Eq.(83) are

$$C_{hWW} = C_{hff} = C_{Wff} = C^V_{Zff} = C^A_{Zff} = 1 \quad , \quad \text{others} = 0\,. \tag{86}$$

In the present model, on the other hand, the prefactors $C_{hXY}(X, Y \neq H_i^\pm)$ in Eq. (83) are given by

$$C_{hWW} = \cos\phi\sin(\beta - \alpha)\,, \tag{87}$$

$$C_{htt} = \frac{y_2 v_{\text{EW}}}{\sqrt{2}m_t} c_L^t s_R^t \cos\alpha\,, \tag{88}$$

$$C_{hbb} = -\frac{y_1 v_{\text{EW}}}{\sqrt{2}m_b} c_L^b s_R^b \sin\alpha\,, \tag{89}$$

$$C_{hTT} = \frac{y_2 v_{\text{EW}}}{\sqrt{2}m_T} s_L^t c_R^t \cos\alpha\,, \tag{90}$$

$$C_{hBB} = -\frac{y_1 v_{\text{EW}}}{\sqrt{2}m_B} s_L^b c_R^b \sin\alpha\,, \tag{91}$$

$$C^L_{hTt} = C^R_{htT} = \frac{y_2}{\sqrt{2}} c_L^t c_R^t \cos\alpha\,, \tag{92}$$

$$C^L_{htT} = C^R_{hTt} = \frac{y_2}{\sqrt{2}} s_L^t s_R^t \cos\alpha\,, \tag{93}$$

$$C^L_{hBb} = C^R_{hbB} = -\frac{y_1}{\sqrt{2}} c_L^b c_R^b \sin\alpha\,, \tag{94}$$

$$C^L_{hbB} = C^R_{hBb} = -\frac{y_1}{\sqrt{2}} s_L^b s_R^b \sin\alpha\,, \tag{95}$$

and $C_{WXY,ZXY}$ in Eq.(83) are read off from Table V in the Appendix A as

$$C_{Wff} = \begin{cases} c_L^t c_L^b & \text{for } Wtb \\ 1 & \text{for other light fermions} \end{cases}, \tag{96}$$

$$C_{Zff}^V = \begin{cases} 1-(s_L^t)^2/(2\hat{v}_t) & \text{for } f=t \\ 1-(c_L^t)^2/(2\hat{v}_t) & \text{for } f=T \\ 1+(s_L^b)^2/(2\hat{v}_b) & \text{for } f=b \\ 1+(c_L^b)^2/(2\hat{v}_b) & \text{for } f=B \end{cases}, \tag{97}$$

$$C_{Zff}^A = \begin{cases} (c_L^t)^2/(2\hat{a}_t) & \text{for } f=t \\ (s_L^t)^2/(2\hat{a}_t) & \text{for } f=T \\ -(c_L^b)^2/(2\hat{a}_t) & \text{for } f=b \\ -(s_L^b)^2/(2\hat{a}_t) & \text{for } f=B \end{cases}, \tag{98}$$

$$C_{ZTt}^L = \frac{1}{2}c_L^t s_L^t \quad , \quad C_{ZTt}^R = 0\,, \tag{99}$$

$$C_{ZBb}^L = -\frac{1}{2}c_L^b s_L^b \quad , \quad C_{ZBb}^R = 0\,. \tag{100}$$

Here we show only couplings which involve the third family quarks and their vector-like partners. For other fermions (leptons,first and second family quarks), the couplings are the same as the SM case. Finally, the coupling term proportional to $C_{hH_i^\pm H_i^\pm}$ in Eq.(83) is derived from the potential $V(\Phi_1,\Phi_2,\Phi_{\rm TC})$ in Eq.(10). Its expression is lengthy, and we do not write it explicitly.

By using Eqs.(83)-(100), we evaluate the decay width of h^0. Like the SM-higgs boson, also h^0 generally decays into $WW/ZZ, \bar{f}f$ via two body decay, WW^*/ZZ^* via three body decay and $\gamma\gamma, gg, Z\gamma$ via loop processes. The relevant decay widths are collected in the Appendix B. Applying these results, we now discuss the production cross section and the signal strengths of the lightest higgs boson in the present model. First, we consider the production cross sections. The cross section of gluon fusion process of higgs boson production $\sigma_{\rm ggF}(h)$ is enhanced compared with the SM case as

$$r_{\rm ggF} \equiv \frac{\sigma_{\rm ggF}[\rm TSSTC]}{\sigma_{\rm ggF}[\rm SM]} = \frac{\Gamma(h\to gg)[\rm TSSTC]}{\Gamma(h\to gg)[\rm SM]} \simeq 2.3-2.8\,, \quad (\text{for } 0.1 \le \epsilon_b \le 1) \tag{101}$$

since C_{htt} in Eq.(88) becomes large; $C_{htt} \simeq 2$. Note that although there are vector-like fermions in the present model, their couplings with the higgs boson, $C_{hTT,hBB}$ in Eq.(90) and (91), are very small due to $c_L^t, c_L^b \simeq 1$ as seen from Fig.5(a-2),(c-2). This means, that vector-like fermions do not give a large contribution to the loop process $gg \to h, h \to gg/\gamma\gamma/Z\gamma$ in the present model. This result is different from results in a model including vector-like quarks e.g.[47]. On the other hand, the cross section of vector boson fusion process (VBF) and vector boson associated process (WH/ZH) of higgs boson production are suppressed compared with the SM case as

$$r_{\rm VBF} \equiv \frac{\sigma_{\rm VBF}[\rm TSSTC]}{\sigma_{\rm VBF}[\rm SM]} = \frac{\Gamma(h\to WW^*/ZZ^*)[\rm TSSTC]}{\Gamma(h\to WW^*/ZZ^*)[\rm SM]} \simeq 0.1\,, \quad (\text{for } 0.1 \le \epsilon_b \le 1)\,, \tag{102}$$

$$r_{\rm WH/ZH} \equiv \frac{\sigma_{\rm WH/ZH}[\rm TSSTC]}{\sigma_{\rm WH/ZH}[\rm SM]} = \frac{\Gamma(h\to WW^*/ZZ^*)[\rm TSSTC]}{\Gamma(h\to WW^*/ZZ^*)[\rm SM]} \simeq 0.1\,, \quad (\text{for } 0.1 \le \epsilon_b \le 1)\,. \tag{103}$$

This suppression arises since these ratios mainly depend on C_{hWW} in Eq.(87), which shows that $C_{hWW} \propto \cos\phi$, and hence becomes small if $\tan\phi$ becomes large. Thus we obtain the ratio of total higgs boson production cross sections for $0.1 \le \epsilon_b \le 1$ as

$$\frac{\sigma[\rm TSSTC]}{\sigma[\rm SM]} \equiv \frac{r_{\rm ggF}\cdot\sigma_{\rm ggF}[\rm SM] + r_{\rm VBF}\cdot\sigma_{\rm VBF}[\rm SM] + r_{\rm WH}\cdot\sigma_{\rm WH}[\rm SM] + r_{\rm ZH}\cdot\sigma_{\rm ZH}[\rm SM]}{\sigma_{\rm ggF}[\rm SM]+\sigma_{\rm VBF}[\rm SM]+\sigma_{\rm WH}[\rm SM]+\sigma_{\rm ZH}[\rm SM]} \simeq 2-2.5\,, \tag{104}$$

where we have used values of $\sigma[\rm SM]$ for $m_h = 126\,\rm GeV$ from [46]: $\sigma_{\rm ggF}[\rm SM] = 15.08$(pb), $\sigma_{\rm VBF}[\rm SM] = 1.199$(pb), $\sigma_{\rm WH}[\rm SM] = 0.5576$(pb) and $\sigma_{\rm ZF}[\rm SM] = 0.3077$(pb).

Next, we consider the signal strength μ_X, which is defined as

$$\mu_X \equiv \frac{\sigma[\mathrm{TSSTC}]}{\sigma[\mathrm{SM}]} \times \frac{\mathrm{Br}(h \to X)}{\mathrm{Br}(h^{\mathrm{SM}} \to X)} \,, \tag{105}$$

for $X = \gamma\gamma/WW^*/ZZ^*/\tau^+\tau^-$ and

$$\mu_{bb} \equiv \frac{r_{\mathrm{WH}} \cdot \sigma_{\mathrm{WH}}[\mathrm{SM}] + r_{\mathrm{ZH}} \cdot \sigma_{\mathrm{ZH}}[\mathrm{SM}]}{\sigma_{\mathrm{WH}}[\mathrm{SM}] + \sigma_{\mathrm{ZH}}[\mathrm{SM}]} \times \frac{\mathrm{Br}(h \to b\bar{b})}{\mathrm{Br}(h^{\mathrm{SM}} \to b\bar{b})} \,, \tag{106}$$

for $X = b\bar{b}$. We note that $\mu_{\tau\tau}[\mathrm{TSSTC}] = 0$ in the present model since the higgs boson does not couple to leptons (see Eq.(9)). This fact is different from the SM higgs boson case. For reference, we list the LHC results of μ_X:

$$\begin{aligned}
\mu_{\gamma\gamma} &= 1.8 \pm 0.5 && (\mathrm{ATLAS}\ 7\,\mathrm{TeV} + 8\,\mathrm{TeV}\ [1])\,, \\
\mu_{WW^*} &= 1.3 \pm 0.5 && (\mathrm{ATLAS}\ 7\,\mathrm{TeV} + 8\,\mathrm{TeV}\ [1])\,, \\
\mu_{ZZ^*} &= 1.4 \pm 0.6 && (\mathrm{ATLAS}\ 7\,\mathrm{TeV} + 8\,\mathrm{TeV}\ [1])\,, \\
\mu_{bb} &= 0.46 \pm 2.18 && (\mathrm{ATLAS}\ 7\,\mathrm{TeV}\ [5])\,, \\
\mu_{\tau\tau} &= 0.45 \pm 1.8 && (\mathrm{ATLAS}\ 7\,\mathrm{TeV}\ [5])
\end{aligned} \tag{107}$$

for $m_h = 126.5\,\mathrm{GeV}$ at the ATLAS group,

$$\begin{aligned}
\mu_{\gamma\gamma} &= 1.56 \pm 0.43 && (\mathrm{CMS}\ 7\,\mathrm{TeV} + 8\,\mathrm{TeV}\ [48])\,, \\
\mu_{WW^*} &= 0.38 \pm 0.56/0.98 \pm 0.71 && (\mathrm{CMS}\ 7\,\mathrm{TeV}/8\,\mathrm{TeV}\ [5])\,, \\
\mu_{ZZ^*} &= 0.7 \pm 0.4 && (\mathrm{CMS}\ 7\,\mathrm{TeV} + 8\,\mathrm{TeV}\ [49])\,, \\
\mu_{bb} &= 0.59 \pm 1.17/0.41 \pm 0.94 && (\mathrm{CMS}\ 7\,\mathrm{TeV}/8\,\mathrm{TeV}\ [5])\,, \\
\mu_{\tau\tau} &= 0.62 \pm 1.13/-0.72 \pm 0.97 && (\mathrm{CMS}\ 7\,\mathrm{TeV}/8\,\mathrm{TeV}\ [5])
\end{aligned} \tag{108}$$

for $m_h = 125\,\mathrm{GeV}$ at the CMS group. From Eqs.(107) and (108), we find that $\mu_{\tau\tau}[\mathrm{TSSTC}] = 0$ is consistent with the present LHC results.

In Fig.10 (a), we show the signal strength μ_X as a function of ϵ_b. In Fig.10 (a), the blue solid, green dotted, red dashed and magenta dot-dashed curves correspond to $\mu_{\gamma\gamma}, \mu_{WW^*}, \mu_{ZZ^*}, \mu_{bb}$, respectively. Moreover, for comparison, we present the values of $\mu_{\gamma\gamma, ZZ^*, WW^*}$ corresponding to the results reported by the ATLAS and CMS experiments and given in Eqs.(107) and (108). From Fig.10 (a), we find $\epsilon_b = 0.7 - 0.93$ is favored by the experimental data on μ_{WW^*, ZZ^*} When ϵ_b becomes large, s_R^b becomes small. Consequentially, C_{hbb} in Eq.(89) becomes small and $\mathrm{Br}(h \to b\bar{b})$ becomes small for large ϵ_b. This fact causes the enhancement of $\mathrm{Br}(h \to WW^*/ZZ^*)$ for large ϵ_b. For $\epsilon_b = 0.7 - 0.93$, we obtain $\mu_{bb} = 0.12 - 0.04$ which is smaller than the SM higgs boson case but still consistent with the LHC results. However, the $\mu_{\gamma\gamma}$ remains smaller than the LHC results even if we take into account the effect of ϵ_b.

To conclude this section, we discuss a possibility of enhancing $\mu_{\gamma\gamma}[\mathrm{TSSTC}] \simeq 2$ while retaining the features of the other channels. For this purpose, there are three possibilities :

1. Adding new vector mesons which couple to higgs boson,
2. Adding new fermions which couple to higgs boson,
3. Adding new scalar particles which couple to higgs boson.

Among these possibilities, the first one occurs naturally in the present model, since the topcolor dynamics generates composite vector mesons. Let us denote such color-singlet vector meson isotriplet by $\rho_\mu^\pm$, and assume its mass to satisfy $M_\rho \gg 2m_h$. We add

$$\mathcal{L}_{h\rho\rho} = C_{h\rho\rho}(gM_W) \cdot h\rho^{+\mu}\rho_\mu^- \tag{109}$$

to Eq.(83). In this case $\Gamma(h \to \gamma\gamma)$ changes from Eq.(B6) to

$$\Gamma(h \to \gamma\gamma) = \frac{\alpha^2 g^2}{1024\pi^3} \frac{m_h^3}{M_W^2} \left| C_{hWW} A_1\left(\frac{4M_W^2}{m_h^2}\right) + C_{h\rho\rho} A_1\left(\frac{4M_\rho^2}{m_h^2}\right) + \cdots \right|^2 , \tag{110}$$

where $\cdots$ contain the $A_{1/2,0}$-terms in Eq.(B6). If $M_\rho \gg 2m_h \simeq 2 \times 126\,\mathrm{GeV}$, A_1 can be take to be equal to -7. Then $\Gamma(h \to \gamma\gamma)$ can be enhanced for suitable values of $C_{h\rho\rho}$. Furthermore, this new vector meson does not give any contribution to the other decay channels at the leading order since $\rho^\pm_\mu$ is color-singlet and $M_\rho \gg 2m_h$. In Fig.10(b), we show the signal strength μ_X for $C_{h\rho\rho}$, with $M_\rho = 1\,\mathrm{TeV}$, as a function of ϵ_b. In Fig.10 (b), the blue solid, green dotted, red dashed and magenta dot-dashed curves correspond to $\mu_{\gamma\gamma}, \mu_{WW^*}, \mu_{ZZ^*}, \mu_{bb}$, respectively. For comparison, we again also present the values of $\mu_{\gamma\gamma,ZZ^*,WW^*}$ from the ATLAS and CMS experiments. The dependence of the results on M_ρ is small for $M_\rho \gg 2m_h$ due to the loop function $A_1(x)$. Summarizing, we find that this modification, i.e. adding $\mathcal{L}_{h\rho\rho}$, gives a large contribution to $\Gamma(h \to \gamma\gamma)$ but $\mathrm{Br}(h \to WW^*/ZZ^*/b\bar{b})$ are not affected by this addition. Therefore, from Fig.10, we find that the present model with

$$\epsilon_b = 0.7 - 0.93 \quad \text{and} \quad C_{h\rho\rho} \simeq 0.4\,, \tag{111}$$

is consistent with the experimental constraints and the LHC results of higgs boson search. Future data from the LHC will allow to constrain the model further. Especially interesting will be the fate of the deficit observed in the $\tau\tau$-channel, and which is by definition explained within our model. If a signal in the $\tau\tau$-channel is ultimately observed, the model must be revised to accommodate such a result.

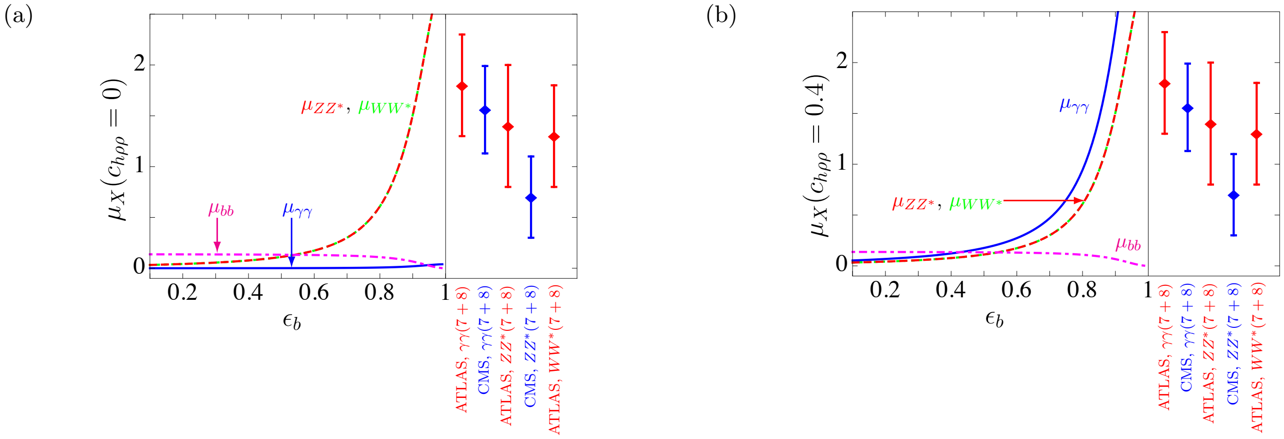

FIG. 10: The signal strength $\mu_X(X = \gamma\gamma, WW^*, ZZ^*, bb)$ as a unction of ϵ_b in the present model. The blue solid, green dotted, red dashed, magenta dot-dashed curves correspond to $\mu_{\gamma\gamma}, \mu_{WW^*}, \mu_{ZZ^*}, \mu_{bb}$, respectively. In both panels, the LHC combined results for $\gamma\gamma$, ZZ^*, WW^* in Eqs.(107,108) are shown together. (a) shows the signal strength for a case with $C_{h\rho\rho} = 0$ and (b) shows the signal strength for a case with $C_{h\rho\rho} = 0.4$ with $M_\rho = 1\,\mathrm{TeV}$

VI. SUMMARY

In this paper we have explored a model where both electroweak symmetry breaking and the origin of the heavy quark masses are due to new strong dynamics. In the model we considered, the third generation quark masses arise from the topcolor interactions via the top-seesaw mechanism. These augment a technicolor sector which is mainly responsible for the generation of the masses of the weak interaction gauge bosons.

The resulting low energy effective theory is a particular three Higgs doublet model. Several novel properties were identified. We considered the CP even scalar state associated with the technicolor sector to be heavy. This assumption is reasonable for the minimalistic technicolor sector we considered, but may be alleviated for other possibilities. In particular, if the technicolor sector is quasiconformal, the scalar state is expected to be light and contribute to the mass eigenstates in the scalar sector.

In the phenomenology analysis of the model we have provided a template on how to confront this type of models with the existing data from the precision electroweak measurements to the recently announced LHC discovery results. In particular we find that a natural way to accommodate the possible observed enhancement in the $h_0 \to \gamma\gamma$ channel, is via the composite vector state which inevitably exist in this type of models.

Our analysis of the model parameter space is to be taken as only illustrative. We have provided the necessary formulas and concepts, shown that viable portion in the parameter space exists and laid out the way for the more detailed scan of the parameter space. The future results from the LHC on the fate of the excess in the $\gamma\gamma$ channel as well as on the deficit in the $\tau\tau$ final states will certainly provide stringent constraints on this type of models.

Appendix A: Results for the analysis of the oblique corrections and δg_L^b

From Eq. (8) in the mass basis of PNGBs and higgses, the following Feynman rules are obtained:

SVV-vertex	Feynman rule
$H^0 Z_\mu Z_\nu$	$i(g/c_W) M_Z \cos\phi \cos(\beta-\alpha) g^{\mu\nu}$
$h^0 Z_\mu Z_\nu$	$i(g/c_W) M_Z \cos\phi \sin(\beta-\alpha) g^{\mu\nu}$
$G^\pm A_\mu W_\nu^\mp$	$igs_W M_W g^{\mu\nu}$
$G^\pm Z_\mu W_\nu^\mp$	$-igs_W^2 M_Z g^{\mu\nu}$
$H^0 W_\mu^+ W_\nu^-$	$igM_W \cos\phi \cos(\beta-\alpha) g^{\mu\nu}$
$h^0 W_\mu^+ W_\nu^-$	$igM_W \cos\phi \sin(\beta-\alpha) g^{\mu\nu}$

TABLE II: Feynman rules for SVV-type vertices for Fig.7(a).

SSV-vertex	Feynman rule
$S^+S^-A^\mu\,,(S=G,H_{1,2})$	$ie(p_+ - p_-)^\mu$
$S^+S^-Z^\mu\,,(\phi=G,H_{1,2})$	$i[g(c_W^2 - s_W^2)/(2c_W)](p_+ - p_-)^\mu$
$G^0H^0Z^\mu$	$-g/(2c_W)\cos\phi\cos(\beta-\alpha)(p_G - p_H)^\mu$
$G^0h^0Z^\mu$	$-g/(2c_W)\cos\phi\sin(\beta-\alpha)(p_G - p_h)^\mu$
$A_1^0H^0Z^\mu$	$-g/(2c_W)[-\sin\zeta_0\sin(\beta-\alpha) - \sin\phi\cos\zeta_0\cos(\beta-\alpha)](p_A - p_H)^\mu$
$A_1^0h^0Z^\mu$	$-g/(2c_W)[\sin\zeta_0\cos(\beta-\alpha) - \sin\phi\cos\zeta_0\sin(\beta-\alpha)](p_A - p_h)^\mu$
$A_2^0h^0Z^\mu$	$-g/(2c_W)[\cos\zeta_0\cos(\beta-\alpha) + \sin\phi\sin\zeta_0\sin(\beta-\alpha)](p_A - p_h)^\mu$
$A_2^0H^0Z^\mu$	$-g/(2c_W)[-\cos\zeta_0\sin(\beta-\alpha) + \sin\phi\sin\zeta_0\cos(\beta-\alpha)](p_A - p_H)^\mu$
$G^\pm H^0W^{\mp\mu}$	$\pm i(g/2)\cos\phi\cos(\beta-\alpha)(p_G - p_H)^\mu$
$G^\pm h^0W^{\mp\mu}$	$\pm i(g/2)\cos\phi\sin(\beta-\alpha)(p_G - p_h)^\mu$
$H_1^\pm H^0W^{\mp\mu}$	$\pm i(g/2)[-\sin\zeta_\pm\sin(\beta-\alpha) - \sin\phi\cos\zeta_\pm\cos(\beta-\alpha)](p_{H^\pm} - p_H)^\mu$
$H_1^\pm h^0W^{\mp\mu}$	$\pm i(g/2)[\sin\zeta_\pm\cos(\beta-\alpha) - \sin\phi\cos\zeta_\pm\sin(\beta-\alpha)](p_{H^\pm} - p_h)^\mu$
$H_2^\pm H^0W^{\mp\mu}$	$\pm i(g/2)[-\cos\zeta_\pm\sin(\beta-\alpha) + \sin\phi\sin\zeta_\pm\cos(\beta-\alpha)](p_{H^\pm} - p_H)^\mu$
$H_2^\pm h^0W^{\mp\mu}$	$\pm i(g/2)[\cos\zeta_\pm\cos(\beta-\alpha) + \sin\phi\sin\zeta_\pm\sin(\beta-\alpha)](p_{H^\pm} - p_h)^\mu$
$G^\pm G^0W^{\mp\mu}$	$-(g/2)(p_{G^\pm} - p_{G^0})$
$H_1^\pm A_1^0W^{\mp\mu}$	$-(g/2)\cos(\zeta_\pm - \zeta_0)(p_{H^\pm} - p_A)$
$H_1^\pm A_2^0W^{\mp\mu}$	$-(g/2)\sin(\zeta_\pm - \zeta_0)(p_{H^\pm} - p_A)$
$H_2^\pm A_1^0W^{\mp\mu}$	$(g/2)\sin(\zeta_\pm - \zeta_0)(p_{H^\pm} - p_A)$
$H_2^\pm A_2^0W^{\mp\mu}$	$-(g/2)\cos(\zeta_\pm - \zeta_0)(p_{H^\pm} - p_A)$

TABLE III: Feynman rules for SSV-type vertices for Fig.7(b). The four-momentum p_i points into the vertex.

Computing the relevant diagrams corresponding to Fig.7, the Peskin-Takeuchi S parameter for the higgs sector in

$SSVV$-vertex	Feynman rule
$S^0S^0Z^\mu Z^\nu\,,(S=h,H,G,A_{1,2})$	$i(g^2/2c_W^2)g^{\mu\nu}$
$S^+S^-Z^\mu Z^\nu\,,(S=G,H_{1,2})$	$i[g^2(c_W^2 - s_W^2)/(2c_W^2)]g^{\mu\nu}$
$S^+S^-A^\mu A^\nu\,,(S=G,H_{1,2})$	$2ie^2g^{\mu\nu}$
$S^+S^-A^\mu Z^\nu\,,(S=G,H_{1,2})$	$i[g^2 s_W(c_W^2 - s_W^2)/c_W]g^{\mu\nu}$
$S^0S^0W^{+\mu}W^{-\nu}\,,(S=h,H,G,A_{1,2})$	$i(g^2/2)g^{\mu\nu}$
$S^+S^-W^{+\mu}W^{-\nu}\,,(S=G,H_{1,2})$	$i(g^2/2)g^{\mu\nu}$

TABLE IV: Feynman rules for $SSVV$-type vertices for Fig.7(c) which contribute to the Peskin-Takeuchi S,T-parameters.

the present model is given by

$$S = \frac{1}{\pi M_Z^2}\left[\begin{array}{l} \cos^2\phi\cos^2(\beta-\alpha)\left\{\begin{array}{l}\mathcal{B}_{00}(M_Z^2,M_Z^2,m_H^2)-\mathcal{B}_{00}(M_Z^2,M_Z^2,m_h^2)\\ -M_Z^2\mathcal{B}_0(M_Z^2,m_H^2,M_Z^2)+M_Z^2\mathcal{B}_0(M_Z^2,m_h^2,M_Z^2)\end{array}\right\}\\ -\mathcal{B}_{00}(M_Z^2,m_{H_1^\pm}^2,m_{H_1^\pm}^2)-\mathcal{B}_{00}(M_Z^2,m_{H_2^\pm}^2,m_{H_2^\pm}^2)-\sin^2\phi\mathcal{B}_{00}(M_Z^2,M_Z^2,m_h^2)\\ +(\sin\zeta_0\sin(\beta-\alpha)+\sin\phi\cos\zeta_0\cos(\beta-\alpha))^2\mathcal{B}_{00}(M_Z^2,m_{A_1}^2,m_H^2)\\ +(\sin\zeta_0\cos(\beta-\alpha)-\sin\phi\cos\zeta_0\sin(\beta-\alpha))^2\mathcal{B}_{00}(M_Z^2,m_{A_1}^2,m_h^2)\\ +(\cos\zeta_0\sin(\beta-\alpha)-\sin\phi\sin\zeta_0\cos(\beta-\alpha))^2\mathcal{B}_{00}(M_Z^2,m_{A_2}^2,m_H^2)\\ +(\cos\zeta_0\cos(\beta-\alpha)+\sin\phi\sin\zeta_0\sin(\beta-\alpha))^2\mathcal{B}_{00}(M_Z^2,m_{A_2}^2,m_h^2)\end{array}\right]. \tag{A1}$$

Similarly, the Peskin-Takeuchi T parameter for the higgs sector in the model is given as

$$T = \frac{1}{4\pi M_W^2 s_W^2}\left[\begin{array}{l} \cos^2(\zeta_\pm-\zeta_0)\left\{B_{00}(0,m_{H_1^\pm}^2,m_{A_1}^2)+B_{00}(0,m_{H_2^\pm}^2,m_{A_2}^2)\right\}\\ +\sin^2(\zeta_\pm-\zeta_0)\left\{B_{00}(0,m_{H_1^\pm}^2,m_{A_2}^2)+B_{00}(0,m_{H_2^\pm}^2,m_{A_1}^2)\right\}\\ +\cos^2\phi\cos^2(\beta-\alpha)\left\{\begin{array}{l}B_{00}(0,M_W^2,m_H^2)-B_{00}(0,M_Z^2,m_H^2)\\ -B_{00}(0,M_W^2,m_h^2)+B_{00}(0,M_Z^2,m_h^2)\end{array}\right\}\\ -\sin^2\phi\left\{B_{00}(0,M_W^2,m_h^2)-B_{00}(0,M_Z^2,m_h^2)\right\}\\ -M_W^2\cos^2\phi\cos^2(\beta-\alpha)\left\{B_0(0,m_H^2,M_W^2)-B_0(0,m_h^2,M_W^2)\right\}\\ +M_Z^2\cos^2\phi\cos^2(\beta-\alpha)\left\{B_0(0,m_H^2,M_Z^2)-B_0(0,m_h^2,M_Z^2)\right\}\\ -\frac{1}{2}\left\{A_0(m_{H_1^\pm}^2)+A_0(m_{H_2^\pm}^2)\right\}\\ +(\sin\zeta_\pm\sin(\beta-\alpha)+\sin\phi\cos\zeta_\pm\cos(\beta-\alpha))^2B_{00}(0,m_{H_1^\pm}^2,m_H^2)\\ +(\sin\zeta_\pm\cos(\beta-\alpha)-\sin\phi\cos\zeta_\pm\sin(\beta-\alpha))^2B_{00}(0,m_{H_1^\pm}^2,m_h^2)\\ +(\cos\zeta_\pm\sin(\beta-\alpha)-\sin\phi\sin\zeta_\pm\cos(\beta-\alpha))^2B_{00}(0,m_{H_2^\pm}^2,m_H^2)\\ +(\cos\zeta_\pm\cos(\beta-\alpha)+\sin\phi\sin\zeta_\pm\sin(\beta-\alpha))^2B_{00}(0,m_{H_2^\pm}^2,m_h^2)\\ -(\sin\zeta_0\sin(\beta-\alpha)+\sin\phi\cos\zeta_0\cos(\beta-\alpha))^2B_{00}(0,m_{A_1}^2,m_H^2)\\ -(\sin\zeta_0\cos(\beta-\alpha)-\sin\phi\cos\zeta_0\sin(\beta-\alpha))^2B_{00}(0,m_{A_1}^2,m_h^2)\\ -(\cos\zeta_0\sin(\beta-\alpha)-\sin\phi\sin\zeta_0\cos(\beta-\alpha))^2B_{00}(0,m_{A_2}^2,m_H^2)\\ -(\cos\zeta_0\cos(\beta-\alpha)+\sin\phi\sin\zeta_0\sin(\beta-\alpha))^2B_{00}(0,m_{A_2}^2,m_h^2)\end{array}\right], \tag{A2}$$

where we compute in the 'tHoot-Feynman gauge with dimensional regularization and $A_0, B_{00}, B_0, \mathcal{B}_{00}, \mathcal{B}_0$ are given by

$$A_0(m^2) = m^2\left[\frac{1}{\bar{\epsilon}} + 1 - \ln m^2\right], \tag{A3}$$

$$B_{00}(q^2, m_1^2, m_2^2) = \left(\frac{m_1^2 + m_2^2}{4} - \frac{1}{12}q^2\right)\left(\frac{1}{\bar{\epsilon}} + 1\right) - \frac{1}{2}\int_0^1 dx \Delta \ln \Delta, \tag{A4}$$

$$B_0(q^2, m_1^2, m_2^2) = \frac{1}{\bar{\epsilon}} - \int_0^1 dx \ln \Delta, \tag{A5}$$

$$\Delta \equiv -x(1-x)q^2 + (1-x)m_1^2 + x m_2^2, \tag{A6}$$

$$\frac{1}{\bar{\epsilon}} \equiv \frac{2}{4-d} - \gamma_E + \ln(4\pi), \tag{A7}$$

$$\mathcal{B}_{00}(q^2, m_1^2, m_2^2) \equiv B_{00}(q^2, m_1^2, m_2^2) - B_{00}(0, m_1^2, m_2^2), \tag{A8}$$

$$\mathcal{B}_0(q^2, m_1^2, m_2^2) \equiv B_0(q^2, m_1^2, m_2^2) - B_0(0, m_1^2, m_2^2). \tag{A9}$$

We are computing using dimensional regularization, and we remark that these results are almost the same as the results for the three higgs doublet model. However, the difference is that one higgs doublet among three higgs doublets does not have the CP-even higgs boson; see Eq. (5). This implies that Eqs. (A1) and (A2) have a divergent part proportional to $1/\bar{\epsilon}$ since we treat the TC sector by using the non-linear sigma model.

Note that if we take a limit, $\tan\phi = 0$, $c_1 = c_2 = 0$, i.e. $\cos\zeta_p = 0$, and $m_{S_2}^2 \gg M_Z^2, m_{S_1}^2$, Eqs.(A1,A2) becomes

$$S = \frac{1}{\pi M_Z^2}\left[\begin{array}{l} \cos^2(\beta-\alpha)\left\{\begin{array}{l} \mathcal{B}_{00}(M_Z^2, M_Z^2, m_H^2) - \mathcal{B}_{00}(M_Z^2, M_Z^2, m_h^2) \\ -M_Z^2\mathcal{B}_0(M_Z^2, m_H^2, M_Z^2) + M_Z^2\mathcal{B}_0(M_Z^2, m_h^2, M_Z^2) \\ +\mathcal{B}_{00}(M_Z^2, m_{A_H}^2, m_h^2) \end{array}\right\} \\ -\mathcal{B}_{00}(M_Z^2, m_{H_H^\pm}^2, m_{H_H^\pm}^2) + \sin^2(\beta-\alpha)\mathcal{B}_{00}(M_Z^2, m_{A_H}^2, m_H^2) \end{array}\right], \tag{A10}$$

and

$$T = \frac{1}{4\pi M_W^2 s_W^2}\left[\begin{array}{l} B_{00}(0, m_{H_H^\pm}^2, m_{A_H}^2) - \frac{1}{2}A_0(m_{H_L^\pm}^2) \\ +\cos^2(\beta-\alpha)\left\{\begin{array}{l} B_{00}(0, M_W^2, m_H^2) - B_{00}(0, M_Z^2, m_H^2) \\ -B_{00}(0, M_W^2, m_h^2) + B_{00}(0, M_Z^2, m_h^2) \\ +B_{00}(0, m_{H_H^\pm}^2, m_h^2) - B_{00}(0, m_{A_H}^2, m_h^2) \end{array}\right\} \\ +\sin^2(\beta-\alpha)\left\{B_{00}(0, m_{H_H^\pm}^2, m_H^2) - B_{00}(0, m_{A_H}^2, m_H^2)\right\} \\ -M_W^2\cos^2(\beta-\alpha)\left\{B_0(0, m_H^2, M_W^2) - B_0(0, m_h^2, M_W^2)\right\} \\ +M_Z^2\cos^2(\beta-\alpha)\left\{B_0(0, m_H^2, M_Z^2) - B_0(0, m_h^2, M_Z^2)\right\} \end{array}\right], \tag{A11}$$

which are finite and reproduce the 2HDM results [24, 50] as they should.

The one-loop corrections to δg_L^b are obtained as

$$\begin{aligned} [\delta g_L^b]^{\rm 1loop}_{\rm gauge} = {} & \frac{1}{2}\frac{g^2}{16\pi^2}[c_L^b]^2\Big([c_L^t]^2 C_{01}(m_t^2, M_W^2) + [s_L^t]^2 C_{01}(m_T^2, M_W^2)\Big) + \frac{g^2 c_W^2}{16\pi^2}[c_L^b]^2\Big(C_{001}(m_t^2, M_W^2) + C_{001}(m_T^2, M_W^2)\Big) \\ & -\frac{g^2}{64\pi^2}[c_L^b]^2[s_L^b]^2\left([c_L^t]^2 B(m_t^2, M_W^2) + [s_L^t]^2 B(m_T^2, M_W^2)\right) + \frac{g^2}{64\pi^2}[c_L^b]^2[c_L^t]^2[s_L^t]^2 C_{004}(m_t^2, m_T^2, M_W^2) \\ & -\frac{g s_W^2}{8\pi^2\sqrt{2}}[c_L^b]\cdot\left(m_t M_W[c_L^t][Y_{tb}^G]C_{02}(m_t^2, M_W^2) + m_T M_W[s_L^t][Y_{Tb}^G]C_{02}(m_T^2, M_W^2)\right), \end{aligned} \tag{A12}$$

operator	Coupling strength	operator	Coupling strength
$Z_\mu \bar{t}_L \gamma^\mu t_L$	$\frac{g}{c_W}\left[g_L^t - \frac{1}{2}(s_L^t)^2\right]$	$Z_\mu \bar{b}_L \gamma^\mu b_L$	$\frac{g}{c_W}\left[g_L^b + \frac{1}{2}(s_L^b)^2\right]$
$Z_\mu \left(\bar{t}_L \gamma^\mu T_L + \bar{T}_L \gamma^\mu t_L\right)$	$\frac{g}{c_W}\left[\frac{1}{2}c_L^t s_L^t\right]$	$Z_\mu \left(\bar{b}_L \gamma^\mu B_L + \bar{B}_L \gamma^\mu b_L\right)$	$\frac{g}{c_W}\left[-\frac{1}{2}c_L^b s_L^b\right]$
$Z_\mu \bar{T}_L \gamma^\mu T_L$	$\frac{g}{c_W}\left[g_L^t - \frac{1}{2}(c_L^t)^2\right]$	$Z_\mu \bar{B}_L \gamma^\mu B_L$	$\frac{g}{c_W}\left[g_L^b + \frac{1}{2}(c_L^b)^2\right]$
$Z_\mu \left(\bar{t}_R \gamma^\mu t_R + \bar{T}_R \gamma^\mu T_R\right)$	$\frac{g}{c_W}\left[g_R^t\right]$	$Z_\mu \left(\bar{b}_R \gamma^\mu b_R + \bar{B}_R \gamma^\mu B_R\right)$	$\frac{g}{c_W}\left[g_R^b\right]$
$W_\mu^+ \bar{t}_L \gamma^\mu b_L + \text{h.c.}$	$\frac{g}{\sqrt{2}}\left[c_L^t c_L^b\right]$	$W_\mu^+ \bar{t}_L \gamma^\mu B_L + \text{h.c.}$	$\frac{g}{\sqrt{2}}\left[c_L^t s_L^b\right]$
$W_\mu^+ \bar{T}_L \gamma^\mu b_L + \text{h.c.}$	$\frac{g}{\sqrt{2}}\left[s_L^t c_L^b\right]$	$W_\mu^+ \bar{T}_L \gamma^\mu B_L + \text{h.c.}$	$\frac{g}{\sqrt{2}}\left[s_L^t s_L^b\right]$

TABLE V: $V\bar{f}f$-couplings.

operator	Coupling strength
$G^+ \bar{t}_R b_L + \text{h.c.}$	$Y_{tb}^G = y_2 s_R^t c_L^b \cos\phi \sin\beta + y_{\text{TC}}^t \sin\phi$
$H_L^+ \bar{t}_R b_L + \text{h.c.}$	$Y_{tb}^L = y_2 s_R^t c_L^b (\cos\beta \cos\zeta_\pm + \sin\phi \sin\beta \sin\zeta_\pm) - y_{\text{TC}}^t \cos\phi \sin\zeta_\pm$
$H_H^+ \bar{t}_R b_L + \text{h.c.}$	$Y_{tb}^H = y_2 s_R^t c_L^b (\cos\beta \sin\zeta_\pm - \sin\phi \sin\beta \cos\zeta_\pm) + y_{\text{TC}}^t \cos\phi \cos\zeta_\pm$
$G^+ \bar{T}_R b_L + \text{h.c.}$	$Y_{Tb}^G = y_2 c_R^t c_L^b \cos\phi \sin\beta$
$H_L^+ \bar{T}_R b_L + \text{h.c.}$	$Y_{Tb}^L = y_2 c_R^t c_L^b (\cos\beta \cos\zeta_\pm + \sin\phi \sin\beta \sin\zeta_\pm)$
$H_H^+ \bar{T}_R b_L + \text{h.c.}$	$Y_{Tb}^H = y_2 c_R^t c_L^b (\cos\beta \sin\zeta_\pm - \sin\phi \sin\beta \cos\zeta_\pm)$

TABLE VI: Couplings between charged scalars and left-handed bottom quark.

and

$$
\begin{aligned}
[\delta g_L^b]^{\text{1loop}}_{\text{NGB}} = & -\frac{1}{2}\frac{1}{16\pi^2}\sum_{\{f\}}\sum_{\{h\}}[Y_{fb}^h]^2 C_{01}(m_f^2, M_h^2) - \frac{1}{64\pi^2}[s_L^b]^2 \sum_{\{f\}}\sum_{\{h\}}[Y_{fb}^h]^2 B_{01}(m_f^2, M_h^2) \\
& +\frac{1}{2}\frac{1}{16\pi^2}[s_L^t]^2 \sum_{\{h\}}[Y_{tb}^h]^2 C_{01}(m_t^2, M_h^2) + \frac{1}{2}\frac{1}{16\pi^2}[c_L^t]^2 \sum_{\{h\}}[Y_{Tb}^h]^2 C_{01}(m_T^2, M_h^2)\,, \\
& +\frac{1}{2}\frac{1}{16\pi^2}[s_L^t c_L^t]\sum_{\{h\}}[Y_{tb}^h][Y_{Tb}^h] C_{03}(m_t^2, m_T^2, M_h^2)\,,
\end{aligned}
\tag{A13}
$$

where $\{f\} = t, T$ and $\{h\} = G^\pm, H_L^\pm, H_H^\pm$ and

$$B(m^2, M^2) = -\frac{m^2}{M^2 - m^2} - \frac{m^4}{(M^2 - m^2)^2} \ln \frac{m^2}{M^2} \,, \tag{A14}$$

$$C_{001}(m^2, M^2) = \frac{m^2}{M^2 - m^2} + \frac{m^4}{(M^2 - m^2)^2} \ln \frac{m^2}{M^2} \,, \tag{A15}$$

$$C_{002}(m^2, M^2) = -\frac{m^2}{M^2 - m^2} + \frac{m^2(m^2 - 2M^2)}{(M^2 - m^2)^2} \ln \frac{m^2}{M^2} \,, \tag{A16}$$

$$C_{003}(m_1^2, m_2^2, M^2) = \frac{1}{m_1^2 - m_2^2} \left[\frac{m_1^2(2M^2 - m_1^2)}{m_1^2 - M^2} \ln \frac{m_1^2}{M^2} - \frac{m_2^2(2M^2 - m_2^2)}{m_2^2 - M^2} \ln \frac{m_2^2}{M^2} \right] , \tag{A17}$$

$$C_{004}(m_1^2, m_2^2, M^2) = C_{002}(m_1^2, M^2) + C_{002}(m_2^2) + 2C_{003}(m_1^2, m_2^2, M^2) \,, \tag{A18}$$

$$C_{01}(m^2, M^2) = \frac{m^2}{M^2 - m^2} + \frac{m^2 M^2}{(M^2 - m^2)^2} \ln \frac{m^2}{M^2} \,, \tag{A19}$$

$$C_{02}(m^2, M^2) = \frac{1}{M^2 - m^2} - \frac{m^2}{(M^2 - m^2)^2} \ln \frac{m^2}{M^2} \,, \tag{A20}$$

$$C_{03}(m_1^2, m_2^2, M^2) = \frac{-m_1 m_2}{m_1^2 - m_2^2} \left[\frac{m_1^2}{m_1^2 - M^2} \ln \frac{m_1^2}{M^2} - \frac{m_2^2}{m_2^2 - M^2} \ln \frac{m_2^2}{M^2} \right] . \tag{A21}$$

Appendix B: Decay widths of the lightest CP even scalar in the model

The two body decay width $\Gamma(h \to WW/ZZ/\bar{f}f)$ are given by [51]

$$\Gamma(h \to WW) = |C_{hWW}|^2 \frac{g^2}{64\pi} \frac{m_h^3}{M_W^2} \sqrt{1 - \frac{4M_W^2}{m_h^2}} \left[1 - \frac{4M_W^2}{m_h^2} + \frac{16M_W^4}{m_h^4} \right] , \quad (\text{for } 4M_W^2 \le m_h^2) \,, \tag{B1}$$

$$\Gamma(h \to ZZ) = |C_{hWW}|^2 \frac{g^2}{128\pi} \frac{m_h^3}{M_W^2} \sqrt{1 - \frac{4M_Z^2}{m_h^2}} \left[1 - \frac{4M_Z^2}{m_h^2} + \frac{16M_Z^4}{m_h^4} \right] , \quad (\text{for } 4M_Z^2 \le m_h^2) \,, \tag{B2}$$

$$\Gamma(h \to ff) = |C_{hff}|^2 \frac{3g^2}{32\pi} \frac{m_f^2}{M_W^2} m_h \left[1 - \frac{4m_f^2}{m_h^2} \right]^{3/2} , \quad (\text{for } 4m_f^2 \le m_h^2) \,, \tag{B3}$$

the three body decay width $\Gamma(\phi \to WW^*/ZZ^*)$ are given by [52]

$$\Gamma(h \to WW^*) = |C_{hWW}|^2 \left[3 + C_{Wtb}^2 \right] \frac{g^4 m_h}{512\pi^3} F\left(\frac{M_W}{m_h} \right) , \quad (\text{for } M_W \le m_h \le 2M_W) \,, \tag{B4}$$

$$\Gamma(h \to ZZ^*) = |C_{hWW}|^2 \left[\left(6 - 12 s_W^2 + \frac{152}{9} s_W^4 \right) + 2|C_{Zbb}^V \hat{v}_b|^2 + 2|C_{Zbb}^A \hat{a}_b|^2 \right] \frac{g^4 m_h}{2048\pi^3 c_W^4} F\left(\frac{M_Z}{m_h} \right) , \quad (\text{for } M_Z \le m_h \le 2M_Z) \,, \tag{B5}$$

and the one-loop induced decay width $\Gamma(h \to \gamma\gamma/gg)$ are given by [51]

$$\Gamma(h \to \gamma\gamma) = \frac{\alpha^2 g^2}{1024\pi^3} \frac{m_h^3}{M_W^2} \left| \begin{array}{l} C_{hWW} A_1\left(\frac{4M_W^2}{m_h^2} \right) + \sum_f C_{hff} N_c Q_f^2 A_{1/2} \left(\frac{4m_f^2}{m_h^2} \right) \\ + \sum_{i=1,2} C_{hH_i^\pm H_i^\pm} \frac{M_W^2}{M_{H_i^\pm}^2} A_0 \left(\frac{4m_{H_i^\pm}^2}{m_h^2} \right) \end{array} \right|^2 , \tag{B6}$$

$$\Gamma(h \to gg) = \frac{\alpha_S^2 g^2}{128\pi^3} \frac{m_h^3}{M_W^2} \left| \frac{1}{2} \sum_{t,b,T,B} C_{hff} A_{1/2} \left(\frac{4m_f^2}{m_h^2} \right) \right|^2 , \tag{B7}$$

and $\Gamma(h \to Z\gamma)$ is given by [51, 53]

$$\Gamma(h \to Z\gamma) = \frac{\alpha^2 g^2}{512\pi^3} \frac{m_h^3}{M_W^2} \left[1 - \frac{M_Z^2}{m_h^2}\right]^3 \left| \begin{array}{l} C_{hWW} \dfrac{c_W}{s_W} A_1 \left(\dfrac{4M_W^2}{m_h^2}, \dfrac{4M_W^2}{M_Z^2}\right) \\ + \displaystyle\sum_f C_{hff} C_{Zff}^V \frac{2N_c \hat{v}_f Q_f}{s_W c_W} A_{1/2} \left(\frac{4m_f^2}{m_h^2}, \frac{4m_f^2}{M_Z^2}\right) \\ + \dfrac{g}{c_W} \displaystyle\sum_{f \neq F} \left[\begin{array}{l} \dfrac{4m_f}{m_F^2} \left(C_{hFf}^L C_{ZFf}^L + C_{hFf}^R C_{ZFf}^R\right) \left(3 + 4\ln\dfrac{m_f}{m_F}\right) \\ - \dfrac{4}{m_F} \left(C_{hfF}^L C_{ZFf}^L + C_{hfF}^R C_{ZFf}^R\right) \end{array} \right] \\ + \dfrac{c_W^2 - s_W^2}{c_W s_W} \displaystyle\sum_{i=1,2} C_{hH_i^\pm H_i^\pm} \frac{M_W^2}{M_{H_i^\pm}^2} A_0 \left(\frac{4m_{H_i^\pm}^2}{m_\phi^2}, \frac{4m_{H_i^\pm}^2}{m_Z^2}\right) \end{array} \right|^2, \tag{B8}$$

where the third line in the right hand side of Eq.(B8) is satisfied for $m_F \gg m_f, m_h, M_Z$ [53]. $F(x)$ is given by

$$F(x) = -|1 - x^2| \left(\frac{47}{2}x^2 - \frac{13}{2} + \frac{1}{x^2}\right) + 3(1 - 6x^2 + 4x^4)|\ln x| + \frac{3(1 - 8x^2 + 20x^4)}{\sqrt{4x - 1}} \arccos\left[\frac{3x^2 - 1}{2x^3}\right], \tag{B9}$$

$A_{1,1/2,0}(x)$ are given by

$$A_1(x) = 2 + 3x + 3x(2 - x)f(x)\,, \tag{B10}$$

$$A_{1/2}(x) = 2x\left[1 + (1 - x)f(x)\right]\,, \tag{B11}$$

$$A_0(x) = x[x - f(x)]\,, \tag{B12}$$

and $A_{1,1/2,0}(x, y)$ are given by

$$A_1(x, y) = 4(3 - t_W^2)I_2(x, y) + \left[\left(1 + \frac{2}{x}\right)t_W^2 - \left(5 + \frac{2}{x}\right)\right] I_1(x, y)\,, \tag{B13}$$

$$A_{1/2}(x, y) = I_1(x, y) - I_2(x, y)\,, \tag{B14}$$

$$A_0(x, y) = I_1(x, y)\,, \tag{B15}$$

$$I_1(x, y) = \frac{xy}{2(x - y)} + \frac{x^2 y^2}{2(x - y)^2}\left[f(x) - f(y)\right] + \frac{x^2 y}{(x - y)^2}\left[g(x) - g(y)\right]\,, \tag{B16}$$

$$I_2(x, y) = -\frac{xy}{2(x - y)}\left[f(x) - f(y)\right]\,, \tag{B17}$$

where

$$f(x) = \begin{cases} [\arcsin(1/\sqrt{x})]^2 & \text{for } x > 1 \\ -\dfrac{1}{4}\left[\log\dfrac{1 + \sqrt{1 - x}}{1 - \sqrt{1 - x}} - i\pi\right]^2 & \text{for } x \leq 1 \end{cases}, \quad g(x) = \begin{cases} \sqrt{x - 1}\arcsin(1/\sqrt{x}) & \text{for } x > 1 \\ \dfrac{1}{2}\sqrt{1 - x}\left[\log\dfrac{1 + \sqrt{1 - x}}{1 - \sqrt{1 - x}} - i\pi\right] & \text{for } x \leq 1 \end{cases} \tag{B18}$$

---

[1] G. Aad *et al.* [ATLAS Collaboration], Phys. Lett. B **716**, 1 (2012) [arXiv:1207.7214 [hep-ex]].
[2] S. Chatrchyan *et al.* [CMS Collaboration], Phys. Lett. B **716**, 30 (2012) [arXiv:1207.7235 [hep-ex]].
[3] J. Ellis and T. You, JHEP **1209**, 123 (2012) [arXiv:1207.1693 [hep-ph]].
[4] J. R. Espinosa, C. Grojean, M. Muhlleitner and M. Trott, arXiv:1207.1717 [hep-ph].
[5] J. R. Espinosa, C. Grojean, V. Sanz and M. Trott, arXiv:1207.7355 [hep-ph].
[6] S. Matsuzaki and K. Yamawaki, arXiv:1207.5911 [hep-ph].
[7] D. Elander and M. Piai, arXiv:1208.0546 [hep-ph].
[8] M. T. Frandsen and F. Sannino, arXiv:1203.3988 [hep-ph].
[9] R. S. Chivukula, B. Coleppa, P. Ittisamai, H. E. Logan, A. Martin, J. Ren and E. H. Simmons, arXiv:1207.0450 [hep-ph].

[10] I. Low, J. Lykken and G. Shaughnessy, arXiv:1207.1093 [hep-ph].
[11] B. Coleppa, K. Kumar and H. E. Logan, arXiv:1208.2692 [hep-ph].
[12] E. Eichten, K. Lane and A. Martin, arXiv:1210.5462 [hep-ph].
[13] L. Susskind, Phys. Rev. D **20**, 2619 (1979).
[14] S. Weinberg, Phys. Rev. D **19**, 1277 (1979).
[15] B. Holdom, Phys. Lett. B **150**, 301 (1985).
[16] K. Yamawaki, M. Bando and K. Matumoto, Phys. Rev. Lett. **56**, 1335 (1986).
[17] T. Akiba and T. Yanagida, Phys. Lett. B **169**, 432 (1986).
[18] T. W. Appelquist, D. Karabali and L. C. R. Wijewardhana, Phys. Rev. Lett. **57**, 957 (1986).
[19] F. Sannino and K. Tuominen, Phys. Rev. D **71**, 051901 (2005) [hep-ph/0405209].
[20] D. D. Dietrich, F. Sannino and K. Tuominen, Phys. Rev. D **72**, 055001 (2005) [hep-ph/0505059].
[21] S. Dimopoulos and L. Susskind, Nucl. Phys. B **155**, 237 (1979); E. Eichten and K. D. Lane, Phys. Lett. B **90**, 125 (1980).
[22] B. A. Dobrescu, C. T. Hill, Phys. Rev. Lett. **81**, 2634-2637 (1998). [hep-ph/9712319].
[23] R. S. Chivukula, B. A. Dobrescu, H. Georgi, C. T. Hill, Phys. Rev. **D59**, 075003 (1999). [hep-ph/9809470].
[24] H. J. He, C. T. Hill and T. M. P. Tait, Phys. Rev. D **65**, 055006 (2002) [arXiv:hep-ph/0108041].
[25] H. S. Fukano and K. Tuominen, arXiv:1102.1254 [hep-ph].
[26] H. S. Fukano and K. Tuominen, Phys. Rev. D **85**, 095025 (2012) [arXiv:1202.6296 [hep-ph]].
[27] C. T. Hill, Phys. Lett. B **266**, 419 (1991); G. Buchalla, G. Burdman, C. T. Hill and D. Kominis, Phys. Rev. D **53**, 5185 (1996).
[28] T. Appelquist and C. W. Bernard, Phys. Rev. D **22**, 200 (1980).
[29] A. C. Longhitano, Phys. Rev. D **22**, 1166 (1980).
[30] A. C. Longhitano, Nucl. Phys. B **188**, 118 (1981).
[31] G. C. Branco, P. M. Ferreira, L. Lavoura, M. N. Rebelo, M. Sher and J. P. Silva, Phys. Rept. **516**, 1 (2012) [arXiv:1106.0034 [hep-ph]].
[32] V. A. Miransky, M. Tanabashi and K. Yamawaki, Phys. Lett. B **221**, 177 (1989); V. A. Miransky, M. Tanabashi and K. Yamawaki, Mod. Phys. Lett. A **4**, 1043 (1989).
[33] M. A. Luty, Phys. Rev. D **41**, 2893 (1990).
[34] M. Hashimoto and V. A. Miransky, Phys. Rev. D **81**, 055014 (2010) [arXiv:0912.4453 [hep-ph]].
[35] W. A. Bardeen, C. T. Hill and M. Lindner, Phys. Rev. D **41**, 1647 (1990).
[36] R. S. Chivukula, E. H. Simmons, B. Coleppa, H. E. Logan and A. Martin, Phys. Rev. D **83**, 055013 (2011) [arXiv:1101.6023 [hep-ph]].
[37] H. E. Haber and R. Hempfling, Phys. Rev. D **48**, 4280 (1993) [hep-ph/9307201].
[38] G. Aad *et al.* [ATLAS Collaboration], Phys. Lett. B **708**, 37 (2012) [arXiv:1108.6311 [hep-ex]].
[39] M. E. Peskin, T. Takeuchi, Phys. Rev. Lett. **65**, 964-967 (1990); M. E. Peskin, T. Takeuchi, Phys. Rev. **D46**, 381-409 (1992).
[40] J. Beringer et al. (Particle Data Group), Phys. Rev. D86, 010001 (2012).
[41] A. K. Grant, Phys. Rev. D **51**, 207 (1995) [hep-ph/9410267].
[42] S. Dawson and E. Furlan, Phys. Rev. D **86**, 015021 (2012) [arXiv:1205.4733 [hep-ph]].
[43] J. Bernabeu, A. Pich and A. Santamaria, Phys. Lett. B **200**, 569 (1988).
[44] C. T. Hill, Phys. Lett. B **345**, 483 (1995) [hep-ph/9411426].
[45] W. Loinaz and T. Takeuchi, Phys. Rev. D **60**, 015005 (1999) [hep-ph/9812377].
[46] https://twiki.cern.ch/twiki/bin/view/LHCPhysics/CERNYellowReportPageAt7TeV
[47] A. Azatov, O. Bondu, A. Falkowski, M. Felcini, S. Gascon-Shotkin, D. K. Ghosh, G. Moreau and S. Sekmen, Phys. Rev. D **85**, 115022 (2012) [arXiv:1204.0455 [hep-ph]].
[48] CMS-PAS-HIG-12-015, http://cdsweb.cern.ch/record/1460419/files/HIG-12-015-pas.pdf
[49] CMS-PAS-HIG-12-016, http://cdsweb.cern.ch/record/1460664/files/HIG-12-016-pas.pdf
[50] H. J. He, N. Polonsky and S. f. Su, Phys. Rev. D **64**, 053004 (2001) [arXiv:hep-ph/0102144].
[51] J. F. Gunion, H. E. Haber, G. L. Kane and S. Dawson, Front. Phys. **80**, 1 (2000).
[52] T. G. Rizzo, Phys. Rev. D **22**, 722 (1980); W. -Y. Keung and W. J. Marciano, Phys. Rev. D **30**, 248 (1984).
[53] T. Abe, N. Chen and H. -J. He, arXiv:1207.4103 [hep-ph].